MASS-YIELD VARIATIONS IN THE THERMAL

AND EPI-THERMAL FISSIONS OF ^{239}Pu

MASS-YIELD VARIATIONS IN THE THERMAL

AND EPI-THERMAL FISSIONS OF ^{239}Pu

By

SOO-LOONG TONG, B.Sc.

A Thesis

Submitted to the School of Graduate Studies

in Partial Fulfilment of the Requirements

for the Degree

Doctor of Philosophy

McMaster University

September, 1971

DOCTOR OF PHILOSOPHY (1971)   McMASTER UNIVERSITY
(Chemistry)   Hamilton, Ontario

TITLE: Mass-yield Variations in the Thermal and Epi-thermal Fissions of ^{239}Pu

AUTHOR: Soo-Loong Tong, B.Sc. (Nanyang University, Singapore)

SUPERVISOR: Dr. K. Fritze

NUMBER OF PAGES: xi, 121

ABSTRACT:

Some cumulative mass-yield ratios for thermal to epi-thermal neutron fissions of ^{239}Pu have been measured by nondestructive Ge(Li) spectrometric and radiochemical methods. The mass-yield ratios of ^{85m}Kr, ^{91}Sr–^{91m}Y, ^{92}Sr, ^{97}Nb–^{97}Zr, ^{99m}Tc, ^{103}Ru, ^{105}Ru, ^{131}I, ^{132}Te–^{132}I, ^{133}I, ^{135}I–^{135}Xe, ^{140}Ba–^{140}La, ^{143}Ce and ^{147}Nd for both thermal to epi-Cd and thermal to epi-Sm fissions did not show any significant fluctuations. The yields of ^{72}Zn and ^{166}Dy–^{166}Ho in epi-Sm fission were found to be 30±2% lower than in the fission caused by thermal neutrons. Similarly the yields of ^{115}Cd and ^{112}Pd were found to be lower by 46±2% and 24±3% respectively. The 77 mass chain, measured as both ^{77}Ge and ^{77}As, showed only a very slight, if any, decrease for epi-Cd and epi-Sm fissions as compared with thermal neutron fissions.

The results are consistent with the two-mode-of-fission hypothesis. An attempt has also been made to

correlate the observations with the effect of the spin
states of the fissioning nucleus at the saddle point.

ACKNOWLEDGEMENTS

TABLE OF CONTENTS

TABLE OF CONTENTS (Continued)

LIST OF FIGURES

LIST OF FIGURES (Continued)

LIST OF TABLES

CHAPTER 1

INTRODUCTION

A. General Introduction

The splitting of the atomic nucleus was first discovered by Hahn and Strassmann [1] in 1939 through careful and unambiguous radiochemical identification of barium and lanthanum activities from neutron-bombarded uranium targets. The term 'fission' was proposed by Meitner and Frisch [2] and they gave a qualitative interpretation of the process as the division of an excited uranium nucleus into two fragments of intermediary weights, in analogy with a charged liquid drop in which the repulsive Coulomb forces compete with the attractive surface tension. This was followed by the first theoretical paper of Bohr and Wheeler [3] which described the mechanism of fission in terms of the liquid drop model.

Intensive experimental efforts made during the war years [4] have revealed many of the fission properties as we know them today. Advances in radiochemistry and, particularly in the techniques of nuclear physics in the past two decades have added many detailed features concerning the energetics, and mass and charge distributions of this phenomenon (see reviews (5), (6) and (7)).

1

We list below a few of the more remarkable features for common fissile materials such as ^{235}U and ^{239}Pu. Those relevant to the present work are discussed in the subsequent sections.

Regarding the mass-yield distribution, the asymmetric double-humped nature which indicates the much higher probability for fission into two unequal fragments (of masses ~100 and ~140) than into two nearly equal fragments (~600 to 1 for thermal neutron induced fission of ^{235}U), has been well established and is still puzzling.

Charge distribution data have been correlated and predicted in a strictly empirical way more successfully than the theoretically oriented postulates. There are two aspects to the empirical correlations: First, the most probable charge division for a given mass split can be summarized by the equal charge displacement hypothesis of Glendenin et al.[8]. The hypothesis states that the most probable charges (Zp) for one fission fragment and for its complementary fragment lie an equal number of units away from the beta stability. Second, the distribution in fragment charge for a given mass chain can be approximated by a Gaussian, $\exp \left(-(Z-Z_p)^2/c\right)$, where $c=0.80 \pm 0.14$ according to a recent paper of Walhl et al.[9].

The major part of the fission energy release (180-200MeV) is in the form of kinetic energy of the fragments (~150MeV) with the remainder as fragment deformation and intrinsic excitation energies. The total kinetic energy does not show a linear variation with the fragment mass ratio but rather a maximum

occurs at a mass ratio of 1.2 to 1.3 instead of 1.0. The excitation energy is dissipated mostly in neutron emission after the fragments are separated. The dependence of the neutron yield on fragment mass is rather striking. For near symmetric fission, the lighter fragment has a higher neutron yield than the heavier fragment. The effect is reversed for very asymmetric fission hence giving rise to the famous saw-tooth shape for the prompt-neutron yield distribution.

Theoretical developments on the other hand are briefly introduced below.

The fission of heavy elements such as uranium and plutonium is a many-body problem. An accurate solution of the many-body Schroedinger equation, in principle, will yield all aspects of fission. But this is still formidable in practice because of the limited capacity of even the most advanced computing machines. Various mathematical and physical approximations (models) have been proposed and useful information extracted and compared with experimental observations.

The most extensively studied theory is the liquid drop model which was originated from the monumental work of Bohr and Wheeler [3]. In this model, the potential energy of the charged liquid drop can be split into two terms, the electrostatic energy which pulls the drop apart, and the surface energy which holds it together. As a measure of the fissionability, Bohr and Wheeler [3] introduced the

parameter $x = E_c^0 / 2E_s^0$ where E_c^0 and E_s^0 are the Coulomb and surface energies of the uniformly charged spherical drop with a sharp surface. This is equivalent to $x = (Z^2/A)/(Z^2/A)_{critical}$ where $(Z^2/A)_{critical} = 50.13$ [5]. Thus nuclei with $x \gtrsim 1$ are unstable towards fission.

The division of the drop is described as the transition from a nearly spherical configuration of low energy to another one representing the separated fragments. A typical contour map of the potential energy surface as function of the deformation coordinates, in the liquid drop model calculation, is shown in Fig. 1. The transition is pictured to pass through the saddle point and the configuration at this point is expected to be of special importance in fission theory. The statics of the model as a result of analytic and numerical development mainly from the works of Cohen and Swiatecki [10], and Strutinskii, Lyashchenko and Popov [11], is rather well understood. The saddle point shapes of nuclei with different fissionability parameters (x) are depicted in Fig. 2.

Dynamic consideration was first introduced by Hill and Wheeler [12] in tracing out the shapes of the fissioning nucleus descending from the saddle point to the stage of scission. In recent works, Nix [13] has developed further the dynamics in addition to the statics, statistical mechanics and also some aspects of the quantum mechanics in studying the fission of the nucleus idealized as a nonviscous irrotational
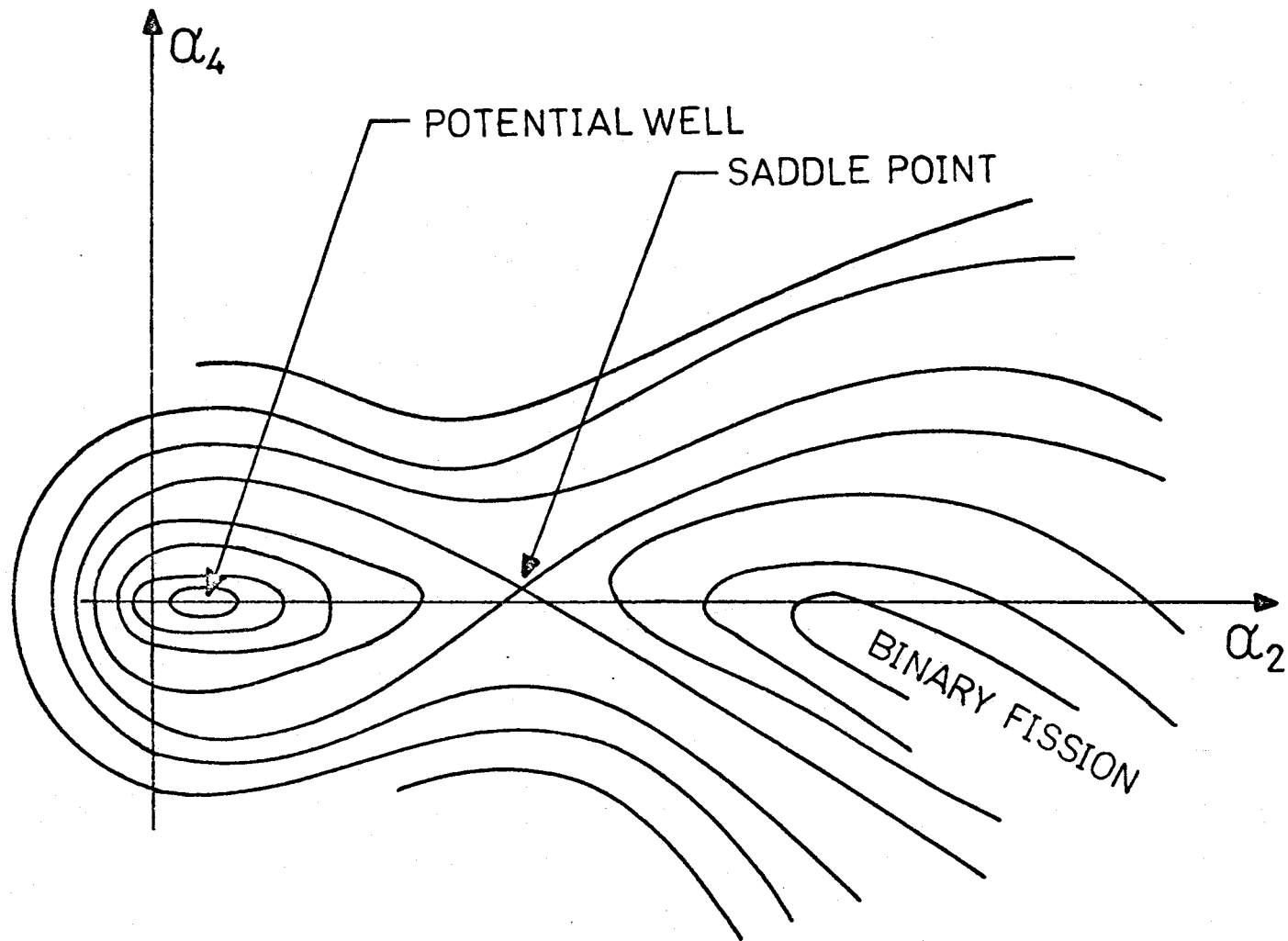
Fig. 1. Schematic Map of the Liquid-drop Distortion Energy as Function of Two Deformation Coordinates.

x=0.0   x=0.3   x=0.4

x=0.5   x=0.6   x=0.7

x=0.8   x=0.9   x=1.0
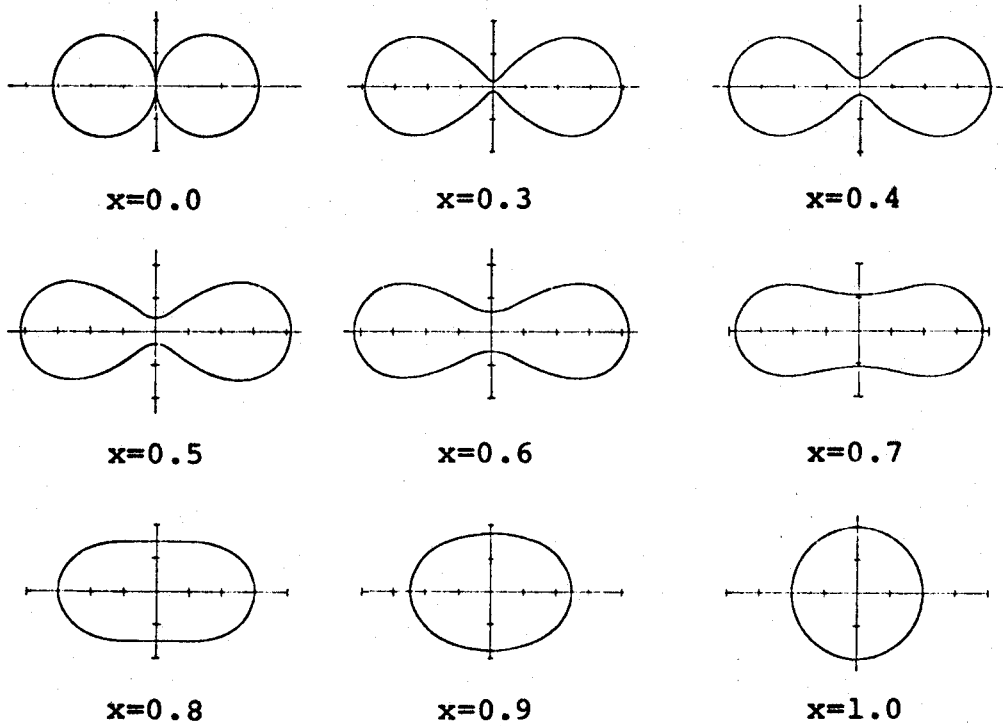
Fig. 2.   Saddle-point Shapes for Various Values of the
Fissionability Parameter x [10].

liquid drop. Though such a calculation is still incapable

of accounting for fission of heavy elements (heavier than about

radium) at low excitation energy, it did reproduce the experimental

fission-fragment mass and energy distributions for fission of

heavy elements at high excitation energy (>40MeV) and medium-

weight nuclei (between about silver and radium) at all excitation

energies.

The inclusion of a shell correction term in the liquid

drop model calculation by Strutinskii [14] which gave rise to

a double-humped fission barrier instead of the conventional

single-peaked shape (see Fig. 3) has been the most remarkable

event in this field for the past few years. The double-

humped fission barrier provides satisfactory explanation for

some anomalous observations of fission, particularly in the

observed fission nuclei isomerism, broad resonance structures

in the fission excitation functions, etc. [15]

So far, the liquid drop model approach still fails to

explain the most striking feature of fission of the heavy

elements such as ^{235}U and ^{239}Pu, namely the asymmetric fission

into two unequal fragments being much more probable than

symmetric fission into two nearly equal fragments.

The statistical model proposed by P. Fong, [16] was

the only one that has given detailed quantitative calculations

and he obtained a mass-yield distribution curve for thermal

neutron induced fission of ^{235}U which agreed well with the

experimental data. Fong assumed that fission is a slow process
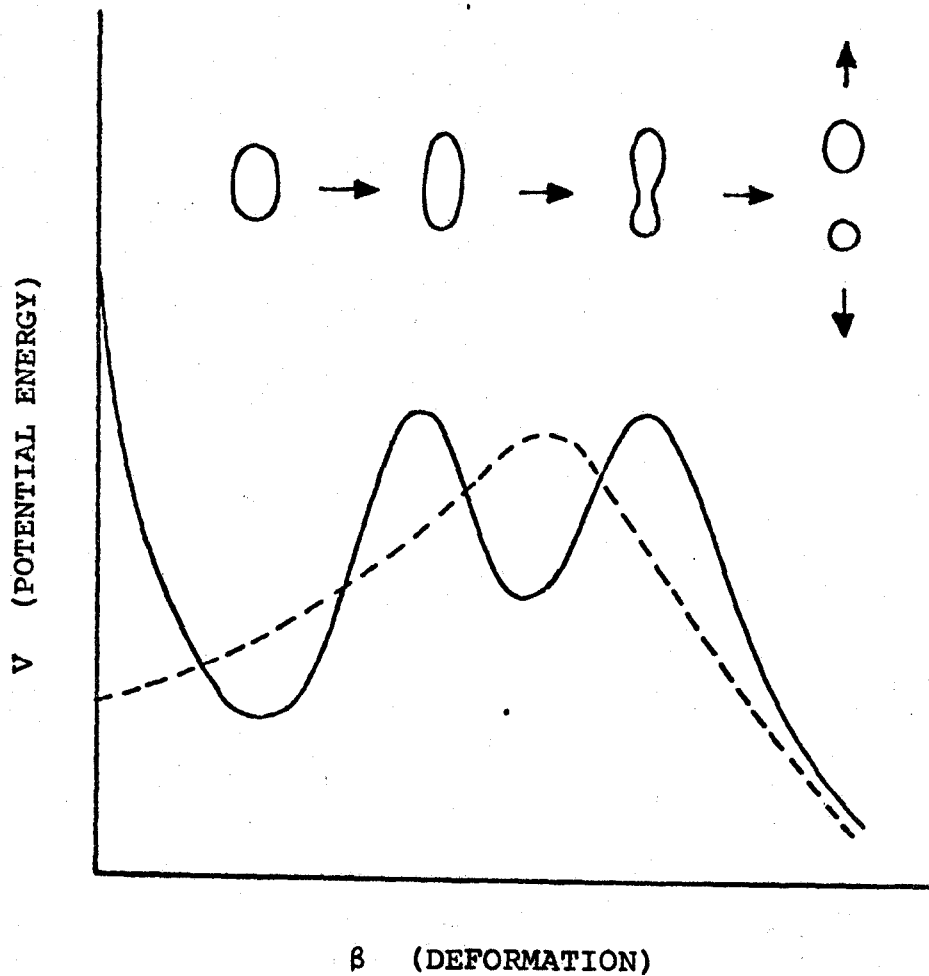
Fig. 3. Schematic illustrations of single-humped (dashed line) and double-humped (solid line) fission barriers. The transition in the shape of the nucleus is schematically represented in the upper part of the figure.

so that equilibrium is established instantaneously at or
near the point of scission. The statistical quantities such
as the mass distribution, are related to the total energy
of excitation of the two nascent fragments at the point
of scission as well as to the level density. The nuclear
level density was examined empirically with shell effects taken
into account. Though this model appears to be complete and free
of arbitrary parameters, later application seems to indicate
that it does not reproduce the experimental data satisfactorily.
When Perring and Storey[17] applied the model to the thermal
fission of ^{239}Pu, a four-humped mass-yield distribution was
obtained. As Fong pointed out more recently, [18] the
application of this model is sensitive to the input parameters
including the nuclear masses, the deformation parameters,
the level density function etc. Therefore more reliable
information on them should be available before the model
may be tested conclusively.

Other models which emphasize the nuclear structure
of the primary fragments at the point of scission as determining
factor on fission fragment distributions include the works of
Brunner and Paul [19], Thomas and Vandenbosch, [20], Ramanna et al[21].
among others.

Another class of theory basically different from the
statistical model is the adiabatic model [22]. According
to this model, the collective deformation is assumed to be slow
compared with the typical period of nucleon motion so that

particle motion can be adjusted adiabatically to the collective
motion of the nuclear surface at the stage of transition
from saddle to scission. The practical nonviscous liquid
drop model calculation as pointed out by Swiatecki [23],
and the channel theory of A. Bohr [24] fall into this class. Bohr's
theory which suggests memory of the saddle-point properties
in the fission process has enjoyed great success especially
in accounting for fission fragment angular anisotropies among
other phenomena. The cluster model of Faissner and Wildermuth[25]
also suggests that the mass and charge distribution may be
determined by nuclear configuration already existing at the
saddle point.

The assumption of equilibrium at or near the point
of scission and the principle of memory of the saddle-point
properties in fission process are contradictory to each other
but both achieved a remarkable measure of success. Griffin[26]
proposed in the Second Symposium on the Physics and Chemistry
of Fission (1969),that rapid collective motion during the
late stages of fission may lead to memory of the saddle-
point properties but not realizing the equilibrium in the mean
time. An appreciable amount of contributions in this regard
can also be found in the same symposium. However, no theory
as yet has been able to account for all aspects of the complicated
phenomenon.

B. The Nature of Fission

Fission is regarded as a nuclear deexcitation process com-

peting with other modes of decay (emission of α,β,γ or other nuclear particles) whenever the nucleus is excited with sufficient energy to overcome the fission energy barrier. In those cases where the fission barrier is sufficiently low, tunnelling from the ground state leads to spontaneous fission.

Excitation of the nucleus may be through compound nucleus interaction with photons, neutrons, positively charged particles, mesons etc., or through direct interaction such as (d,p), (α,α')etc.. Many targets from about silver up to the heaviest man-made elements have been reported to undergo fission. The typical and most extensively studied are the low energy neutron fissions of ^{233}U, ^{235}U and ^{239}Pu and fast neutron fissions of ^{232}Th and ^{238}U.

It is generally assumed that the fission process takes place in sequential stages, though no definite boundaries have been set between stages. The following discussion mainly refers to typical low energy neutron induced fission. However, though the lifetime for fission is related to the excitation energy, the fission mechanism at different excitation energies is in many ways quite similar.

The first stage is the formation of the compound nucleus. The excitation energy in the form of the binding energy and kinetic energy of the incident neutron is shared among the nucleons.

The second stage is the crossing of the saddle point. The surface energy increases initially with deformation but the

Coulomb energy decreases. The Coulomb energy decreases faster than the increase in surface energy for large deformation so that at intermediate deformations there exist some transition states. They are usually designated as fission channels, each with one or a few modes of motion.

The passage over the deformed saddle shape is the rate-determining step and the time required can be estimated from the observed sizes of the fission widths of resonances as about 10^{-14} to 10^{-12} sec.

The next stage is the transition from the saddle shape to the point of scission, which is defined as the point beyond which no nuclear interaction between the fragments exists. The time taken has been estimated to be $\sim 10^{-21}$-10^{-20} sec.[18]. When the scission point has been reached, the fragment mass and charge distributions are established.

The scission process may involve a violent snapping action, permitting the release of some of the prompt neutrons, and sometimes a light charged particle, most probably an alpha-particle in between the two separating fragments [27]. This is known as ternary fission; typically the most probable α-ternary fission is about one four-hundredth of the binary fission for thermal neutron-induced fission of ^{235}U [28].

After scission, the nascent fragments, usually called primary fission fragments, are highly deformed in shape and they possess little kinetic energy at the first instant.

The fragments accelerate apart under the long range Coulomb interaction, taking approximately 10^{-20} sec to reach 90% of the final kinetic energy, in the range of 50 to 105 MeV. Fission characteristics of interest that can be measured at this stage include primary fission fragment mass, kinetic energy and angular distributions.

At a later stage of the separation, the highly deformed fragments reorient themselves and emit most or all of the prompt neutrons, prompt fission gamma-rays and conversion-electron radiations. The times required for the prompt neutron and gamma-emission are 10^{-15} - 10^{-18} and $\sim 10^{-11}$ sec respectively. The prompt neutron and gamma emission yields as a function of fragment mass and the kinetic energy distribution provide useful information about the fission energetics.

Finally, the primary fission products (to be distinguished from primary fission fragments before neutron and gamma emissions) being far removed from the beta stability line will undergo sequential beta decays, accompanied by delayed gamma and conversion-electron, and characteristic x-rays emissions. This process is slow and has a life-time $\geq 10^{-3}$ sec. Delayed neutron emission which is of crucial importance to nuclear reactor design arises following beta-decays of some primary fission products which lead to highly excited intrinsic states where neutron emission competes with further β or γ-deexcitation.

If in a given mass chain the yields of nuclides with

different atomic number were measured before any beta decay, they
are known as the independent yields and reflect the charge
distribution in the process of fission.

After sequential beta decays, the yield of the end
product is called the cumulative yield of the mass chain. The
cumulative mass-yield distribution is also expected to hinge
on the nature of the mass splitting mechanism.

Since radiochemical studies of the cumulative mass-
yield is of prime concern to the present work, the following
is contributed as a review of this field.

C.   The Radiochemical Studies of Cumulative Mass-Yield Distribution

1.   Radiochemical method

The common binary fission yields a spectrum of fission
products of masses ranging from ~70 to ~170. Cumulative
mass yield of a specific nuclide may be determined by chemical
separation at the time all its precursors have undergone
sequential beta decays, or when the parent and daughters are
in a state of transient equilibrium.

At the beginning, a measured amount of the non-
radioactive element known as carrier of the specific nuclide
of interest is added to the solution of the fissile material
and its fission products. It is essential that isotopic

exchange is completed between the stable and radioactive
isotopes of the element. Conventional analytical procedure
are then employed to separate the element from the fissile
material and the gross fission products in a state of radio-
chemical purity. The beta or gamma radiations of the sample
are measured with radio counting instruments to identify the
isotope and determine the amount of the radioactive species.
The chemical yield which was determined by some quantitative
method should equal the percentage recovery of the isotope
under investigation. Hence the fission yield of the specific
isotope can be calculated from the counting data, the chemical
yield and the known number of fission of the sample.

2. Cumulative mass-yield distribution

The mass-yield distributions of ^{233}U, ^{235}U, ^{239}Pu, ^{232}Th,
^{238}U etc. have been well studied by this method. Fig. 4 shows
the typical cumulative mass-yield distribution curves of the
thermal neutron-induced fissions of ^{235}U and ^{239}Pu, and the fast
neutron fission of ^{232}Th.

For common fissile nuclides it is most striking that
the mass-yield distributions are asymmetric in shape. The
most probable heavy fragment mass number is 139, and the most
probable light fragment mass number is found to vary from 94
to 100, according to the mass number of the target nuclide.
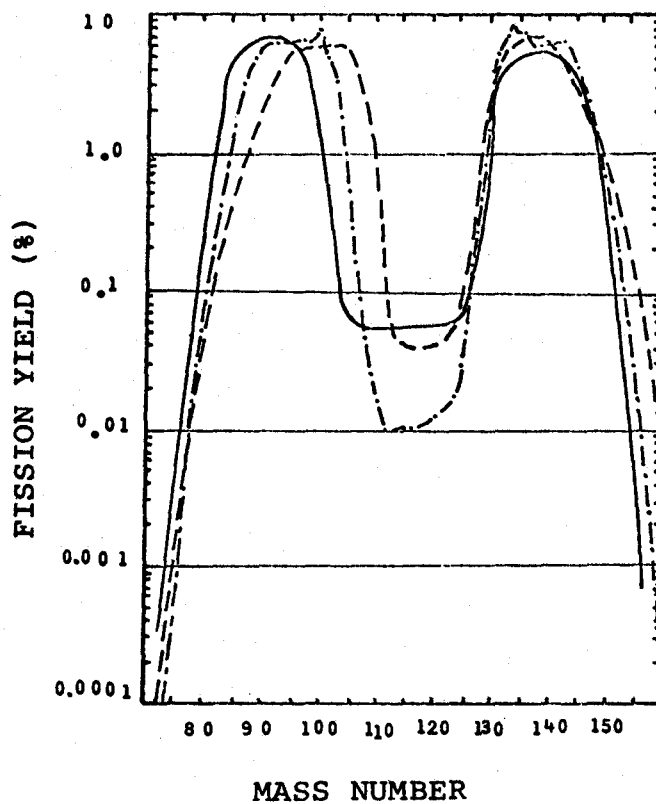
Fig. 4. Typical fission mass-yield distribution curves:
———— for ^{232}Th(fast n, f); —.—.—.— for ^{235}U
(thermal n, f); — — — — for ^{239}Pu(thermal n, f).

The peak-to-valley mass-yield ratios for thermal neutron fissions ^{235}U and ^{239}Pu are 650 and 150 respectively.

Mass spectrometric techniques have also been applied in the studies of mass-yield distribution [30]. Fine structure was found in the thermal neutron fission of ^{235}U, for example, where the yield of ^{134}Xe was anomalously higher than expected from the smooth mass-yield distribution curve obtained by earlier radiochemical measurements.

The mass-yield distribution changes as a function of the mass number of the fissioning nucleus as well as a function of the excitation energy in the system. The general trends derived from experimental observed results can be summarized in Fig. 5.

The fission of heavy (Z $\geqslant$ 90) elements is predominantly asymmetric. The symmetric valley in the mass-yield distribution curve is virtually undectectable for spontaneous fission. But as the excitation energy of the fissioning nucleus is increased it begins to fill in. At high excitation, the situation is obscured because the later chanoe fission after emitting one or a few neutrons may contribute significantly. For excitation energies between the threshold and ~20MeV, very asymmetric fission yields in the wing regions of the mass yield curve increase in similar trend as the symmetric fission, according to the compilation of Katcoff [29] and also data reported by Levy et al. [31] and Borisova et al. [32].
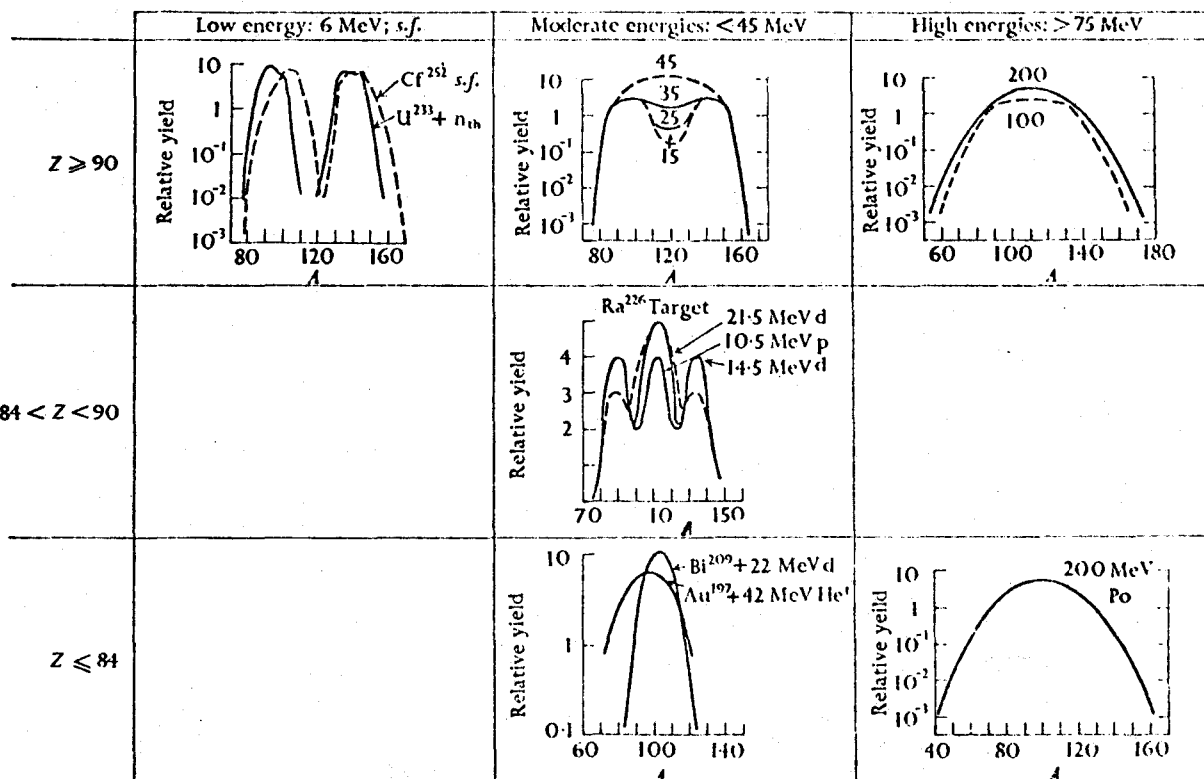
Fig. 5. The dependence of fragment mass-yield on excitation energy and the target atomic number. (From Wilets[22])

The intermediate mass fissioners such as actinum and radium show a symmetric peak coexisting with the asymmetric peaks for near threshold fission [33]. Asymmetric fission diminishes at higher excitation.

The lighter fission elements ($z < 84$) exhibit predominantly symmetric fission distribution [33] which has also been found to broaden with increasing excitation energy.

D. The Two-mode-of-fission Hypothesis

Speculative attempts have been made to account for the observed trends in mass yield distribution curves. One of these is the two-mode-of-fission hypothesis proposed by Turkevich and Niday [34] in explaining a rather flat region observed in symmetric fission of ^{232}Th induced by fast neutrons. According to this hypothesis, there are two independent modes for fission: one associated with symmetric and one with asymmetric mass distributions.

Fairhall et al. [33] defined the two-mode of fission on a different basis in view of the characteristic energy dependence and the lack of A (mass number) dependence of the symmetric fission in uranium and plutonium compound nuclei, coupled with the observation of the triple-peaked mass yield distribution curve of radium. They assumed that the symmetric mode corresponds to low excitation which occurs when fission takes place after the emission of one or more neutrons from the compound

nucleus, and the asymmetric mode corresponds to primary fission
of the compound nucleus at higher excitation energy. Decomposition
of the mass yield curve into the two modes in several cases seems to
be in satisfactory agreement with the hypothesis, e.g. ^{233}U fission with
^{4}He of energies ranging from 25.3 MeV to 40.5 MeV by Colby et al. [35];
^{232}Th + pile neutrons by Iyer et al. [36] and also the work of Britt
et al. [37] The latter authors were also able to correlate the
character of total kinetic energy release as a function of mass split
with the two fission modes.

Ford [38] developed a statistical test of the two-mode
of fission hypothesis for experimentally observed mass-yield
data in terms of linear algebra analysis. He regarded the
two-mode hypothesis as implying that for a given target and
projectile there are two and only two configurations for the
compound nucleus that may result in fission. For each configuration
there correspond many possible mass yields in different frequencies
which can be represented by a vector as a whole. The total mass
yield curve is a result of the combination of two linearly independent
vectors. The variations of the mass yield distribution as a function
of excitation energy is due to the change in proportions of the two
configurations.

The statistical tests on fission yields from proton-induced
fission of ^{232}Th, proton-induced fission of ^{238}U, α - particle
induced fission of ^{238}U, and deuteron-induced fission of
natural uranium did give reasonably high levels of significance

for accepting the hypothesis [38]. Similar tests carried out by Levy et al. [31] for neutron-induced fission of ^{235}U and ^{238}U showed general agreement except for thermal neutron induced fission. Continuing this work [39] the authors found deviations at higher excitation energies for some mass numbers. It was thought that multi-chance fissions following emission of one or more neutrons might perturb the results. Fission before neutron emission is called first-chance, after the emission of one neutron is called second-chance, and so on. Hence in a later work, Ford and Leachman [40] have taken this into account. The observed yields and the first-chance yields for ^{236}U compound nucleus, and also the observed yields for neutron-induced fission of ^{232}Th and ^{238}U, were found in good agreement with the hypothesis. Using this method of analysis, Choppin and Meyer [41] also observed consistency with the two-mode hypothesis for their fission yield data of ^{238}U induced by 7.1, 9.4 and 12.0 MeV protons.

A recent speculative interpretation of the mass yield distribution was made by Schmitt and Konecny [42]. They suggested "two-component" instead of the two distinct modes hypothesis such that the symmetric and asymmetric components may arise from different "mechanisms" which may or may not involve separate saddle point states. On the basis of the experimental results of the fragment kinetics of the fission of ^{226}Ra with 13 MeV protons, including fragment energies, masses

and mass-energy distributions, they observed that the properties

of the symmetric fission of radium were quantitatively consistent

with the results of the liquid drop model calculations of Nix and

Swiatecki [43] while the asymmetric fission could be ascribed

to a mechanism determined by the nuclear structure properties

(especially shell structures) of the fragments. For the symmetric

component, the fragments were thought to be formed in softer,

relatively highly deformed configurations characteristic

of a liquid drop. While in the other component, the fragment

shell effect seems to dominate, and the heavier fragments are

formed in less highly deformed configurations.

The two-mode hypothesis derived from fission well above

threshold energy has also been invoked in interpreting mass

yield variations of fissions induced by resonance neutrons.

Variations have been observed in the mass yield ratios

of the asymmetric to symmetric fission fragments of ^{233}U, and

^{235}U and ^{239}Pu for fissions with resonance neutrons. Radio-

chemical studies of such an effect are always measured in

terms of the 'R' value which is defined as:

$$R = \frac{(A_{asym}/A_{sym})_{resonance}}{(A_{asym}/A_{sym})_{thermal}}$$

where A is the corrected activity of a nuclide, subscript 'asym'

refers to an asymmetric fission product (usually ^{99}Mo or ^{140}Ba),

and subscript 'sym' refers to a symmetric fission product

(^{115}Cd, ^{121}Sn, ^{113}Ag, etc.).

The earliest work of the Los Alamos Radiochemistry Group [44] measured the asymmetric to symmetric fission yield ratios for thermal to epi-cadmium neutron-induced fissions of ^{235}U and found a small but significant difference for the two types of fission. Later measurements of Faler and Tromp [45] on ^{235}U with monochromatic neutrons with energy below 2 eV confirmed this effect.

More drastic changes were reported by Regier et al. [46] for the 0.297 eV resonance fission of ^{239}Pu, and "R" value of ~2.4 was found for ^{115}Cd, ^{121}Sn and ^{125}Sn. For all epi-samarium neutron fission, where the majority of the fission events is due to the 0.297 eV resonance, effects of similar magnitude were also reported.

In the "wheel" experiments of Cowan et al. [47] for which atomic bomb explosions were used as neutron sources, fissions of ^{235}U and ^{239}Pu were studied with incident neutron energy ranging from tens to several hundred eV. Their results indicated that the asymmetric to symmetric yield ratios at different resonances can always be classified into two groups: one group was characterized by fission less symmetric than thermal-neutron fission and the other being more symmetric.

Ford and Leachman [40] applied statistical tests on the results of Cowan et al. and found no significant deviation from the two-mode hypothesis.

The idea of the variations in the mass yields of products

from symmetric fission induced by neutrons in the resonance energy region as the competition of the two fission modes seems unable to account for the observation of Croall and Willis [48]. They have found considerable increases in the yields of ^{77}As and ^{78}As accompanying decreases in the yields of products from symmetric fissions in the epi-Cd as compared with thermal neutron fissions of ^{239}Pu. The contrary effect in ^{77}As and ^{78}As should be expected as we notice that for fission at well above threshold energy, the yields of products from very asymmetric fission on the far wings of the mass yield curve change in the same direction as the symmetric fission yields. Indeed a small but significant effect in ^{72}Zn has been found in a study by Fritze [49] in which an ~10% decrease in ^{72}Zn was associated with the decrease in ^{115}Cd for epi-Cd fission as compared with thermal neutron fission.

One of the purposes of this work was to throw some light on such contradictions. Regier et al.[46] had shown that for all epi-Sm neutron fission of ^{239}Pu the effect in the symmetric yields was almost comparable to the largest decrease observed for the 0.297eV resonance. One therefore could expect if there is any effect in the very asymmetric fission yields associated with that observed in the symmetric region for the 0.297eV resonance, study of the epi-Sm fission of ^{239}Pu would be as effective.

The fluctuations in the asymmetric to symmetric yield ratios which indicate that symmetric fission is more favorable

in one group of resonances and less in the other has more often been related to the effect of the level structure of the compound nucleus at the saddle point, as we shall see in the next section.

E. The Effect of the Spin States of the Compound Nucleus at
    The Saddle Point on Fission Mass-Yield Distribution

Consideration of the effect of the spin states of the compound nucleus at the saddle point on post-scission characteristics was based on the channel theory introduced by A. Bohr in 1955[24]. According to Bohr, as the excited nucleus approaches the saddle point (for near threshold excitation), most of the excitation energy is converted to deformation energy. The nucleus is assumed to be "cold" at the saddle point and only a few widely separated quantum levels representing the motion are available. These levels are restricted to low energy vibrations and rotations similar to those which the compound system would exhibit near its ground state. Bohr assumed that some of the properties of the quantum states remain good quantum numbers, or otherwise "frozen-in", as the nucleus passes from the saddle point to the point of scission. Therefore one expects that these properties would give rise to some regularities in the post-scission observables. This assumption is basically the assumption of the adiabatic model and its validity depends on the duration of the transition from saddle point to scission. If it is so long that statistical equilibrium

can be attained then the assumption of the statistical model
prevails.

On the basis of Bohr's theory, it is possible to correlate
the experimental fission fragment angular anisotropies with
the level structure of the compound nucleus at the saddle point.
It is generally accepted that the deformed nucleus at the saddle
point is axially symmetric and it may be approximately described
with a quantum number K, defined as the component of the
nuclear angular momentum along the symmetry axis of the nucleus
itself. Bohr's theory predicts that the ultimate fission fragment
direction would be closely related to the available K states
in the transition state nucleus because the nuclear symmetry
axis is assumed to be the axis along which the two fragments
separate. There are numerous experimental works which have
been consistently interpreted in terms of the theory (see (5),
(6) and (7)). In fact, the general agreement between theory
and experimental data on fission fragment angular distribution meas-
urements has been so good that several authors have even used
the theory to extract information on nuclear structure and the
transition states for the saddle point nucleus.

Bohr's theory has been extended to a few other fission
phenomena. Wheeler [50] suggested that the mass yield ratios of
asymmetric to symmetric fission products might differ from re-
sonance to resonance for low energy neutron fissioners, de-
pending on the spin states of the fissioning compound nucleus
at the saddle point. The argument was based on a consideration

of the symmetry characters of the wave function of the fissioning

nucleus at the saddle point and assuming that (i) fission

takes place through only a few lowest-lying fission channels, and

(ii) the symmetry character is a constant of motion for the

transition from saddle to scission. The type of symmetry

character responsible is the octupole deformation which consists

of the mass-asymmetry vibration (or sloshing mode) in which

material is transferred from one end of the prolate body

to the other, and the bending vibration mode. [51]

The spin states for a compound nucleus formed by low

energy (S-wave) neutrons incident on a target nucleus with spin

and parity of I^π can be either $(I + 1/2)^\pi$ or $(I - 1/2)^\pi$. The

possible spin states J^π of the compound nuclei ^{236}U and ^{240}Pu

formed by S-wave neutron absorption are 3^- or 4^-, and 0^+ or 1^+

respectively.

It is believed that for ^{236}U [51] the 3^- levels proceed

through a fully open saddle point channel with one quantum of

of mass-asymmetry vibration (and rotation), for which symmetric

fission will be forbidden. It may also proceed through a

partially or fully open channel corresponding to bending

vibration where symmetric fission is allowed. The latter is

the only open channel possible for the 4^- levels. Consequently,

one expects the average mass yield ratios of asymmetric to

symmetric fission fragments to be larger for the 3^- levels

than for the 4^- levels.

For ^{239}Pu, since the 0^+ resonant states cannot decay

through saddle point channels that contain mass-asymmetry vibration, some symmetric mass division is expected in these resonances. The 1^+ resonant states, as suggested by Griffin[52], are probably a combination state of mass asymmetry and bending vibrations; so symmetric division is expected to be suppressed.

Experimental results of Los Alamos Radiochemistry Group [44], Faler and Tromp [45], Regier et al. [46] and Cowan et al. [47] discussed earlier, have been interpreted satisfactorily in terms of the present theory. The experimental results suggest that for ^{239}Pu the 0.297eV resonant state has spin and parity of 1^+ where symmetric fission is suppressed. In thermal neutron fission, the thermal cross-section is composed of certain amount of contribution from the 0.297eV resonance plus a larger contribution from the negative energy resonance believed to have spin and parity of 0^+.

Other types of experimental evidences in support of Bohr's theory include:

(i) the definite variations of fragment kinetic energy from level to level correlated with the spin states of the compound nucleus as reported by Melkonian and Mehta [53] for ^{235}U and ^{239}Pu.

(ii) the significant variations of the mean number of neutron emitted per fission in a systematic manner among the resonances as observed by Weinstein et al. [54] for ^{233}U, ^{235}U and ^{239}Pu.

The spins for neutron resonances can be directly determined from neutron scattering measurements. Comparisons

of the direct and indirect spin assignments based on Bohr's theory are displayed in Table 1 and Table 2 for ^{235}U and ^{239}Pu respectively. The general agreement shows definite correlations of some of the post-scission characteristics, such as mass-yield and kinetic energy distribution and the neutron multiplicity with the spins of the compound nucleus at the saddle point.

However, the results of Croall and Willis [48] on the mass yield variations of the very asymmetric fission fragments (^{77}As and ^{78}As) for thermal and epi-Cd neutron fission of ^{239}Pu described earlier, are unable to be accounted for with the present theory. In addition, it is worthwhile noting that Popa et al. [63] reported significant fluctuations in the relative yields of asymmetric fission products for thermal and epi-Cd neutron induced fission of ^{235}U. Wheeler's extension of Bohr's theory also seems unalbe to provide a consistent interpretation. As shown by the works of Regier et al. [46] and Faler and Tromp [45], the spin state effect is much larger for ^{239}Pu than for ^{235}U in the variations of the symmetric yields. It is therefore expected that any effect in the asymmetric fission yields that may be related to the spin states of the compound nucleus at the saddle point should be more drastic for ^{239}Pu than for ^{235}U. Another purpose of this work was to investigate carefully such a possibility for the thermal and epi-Cd and epi-Sm fissions of ^{239}Pu.

TABLE 1

^{235}U Resonance Spin (J) Assignments

Resonance Energy (eV)	DIRECT			INDIRECT		
	Asghar et al. (55)	Weigman et al. (56)	Bowman et al. (57)	Cowan et al. (47)	Melkonian & Mehta (53)	Weinstein et al. (54)
6.39	4	4				4
7.08	3	3	3			3
8.79	3		3	(A)$^+$	L$^#$	3
9.29	3	3				
10.20	3					
11.65	4		3			4
12.39	4	4	3			4
15.40	3	3	3	A	H	
16.08	(4)*	3	3	A	H	4
16.69	3	3	3	A		4
18.07	3		3	(A)		4
19.31	4	4		A	H	4
21.08		3		A	H	3
22.39	3	3		A		
22.95			3			3
23.42		4		A	H	
23.65			3			
27.82	3	4		A	H	
30.86		3				
32.07	(4)	4		A	H	
33.53	4	4		A	L	
34.39	4	3		S	L	
35.26	4	4		S	L	
39.41	4	4		S	L	

* Uncertainty of assignments.

+ S = increased symmetric fission, A = decreased symmetric fission.

# L = lower average kinetic energy of fragment,
  H = higher average kinetic energy of fragment.

TABLE 2

^{239}Pu Resonance Spin (J) Assignments

Resonance Energy (eV)	DIRECT				INDIRECT			
	Bollinger (58)	Sauter & Bowman (59)	King & Block (60)	Asghar (61)	Cowan et al. (47)	Melkonian & Mehta (53)	Farrell (62)	Weinstein et al. (54)
0.298	1							1
7.85	1	1						1
10.95	1	1						1
11.9	1	1						1
14.3		1					1	1
14.7	0	1		1			1	1
15.5	0	0			1		0	0
17.7	1	1		1	1		1	1
22.3		1		1	1	1	1	1
23.9							1	1
26.2				1	1	(1)	1	1
32.3		0			(0)*	0	0	0
41.5	0	1	1	1	1	(0)	1	1
44.5	1	1	1	1	1	(1)	1	1
47.6		0		0	1	1	0	0
52.6	1	1	1	1	1	1	1	(0)
62.7							0	0
75.0		1	1	1	1	1	1	1
81.0					0		0	0
90.0			0	1				0

* Parentheses indicate uncertain assignment.

CHAPTER 2

EXPERIMENTAL PROCEDURES

A. Introduction

The variations in the mass yields of several symmetric and very asymmetric products in the epi-thermal fission as compared with thermal fission of ^{239}Pu have been studied in this work by means of radiochemical methods. These nuclides included ^{72}Zn, ^{77}Ge, ^{77}As, ^{112}Pd, ^{115}Cd and ^{166}Ho. High yield products from asymmetric fission have also been investigated by nondestructive Ge(Li) spectroscopic measurements of the gross fission products [64]. Brief information on these nuclides is given below.

The cumulative yield of ^{72}Zn in the thermal neutron induced fission of ^{239}Pu is 1.2×10^{-4}% [29]. This isotope cannot be produced by reactions other than fission. It has a half-life of 46.5 hr and emits gamma-rays of 144.8 keV (90%) and 192.0 keV (10%) with intensities shown in parentheses.

According to Croall and Willis [48], the yield of ^{77}As is 7.3×10^{-3}% in the thermal fission of ^{239}Pu. The branching of the A = 77 mass chain is quite complicated and is illustrated in Fig. 6. About 97% of ^{77}As decays to the ground level of ^{77}Se while the rest is associated with gamma-rays of 239.3 keV (2.5%) and 250.1 keV (0.2%) [66]. Gamma-ray spectra following the decay of ^{77}Ge show a number of gamma transitions, the most prominent ones
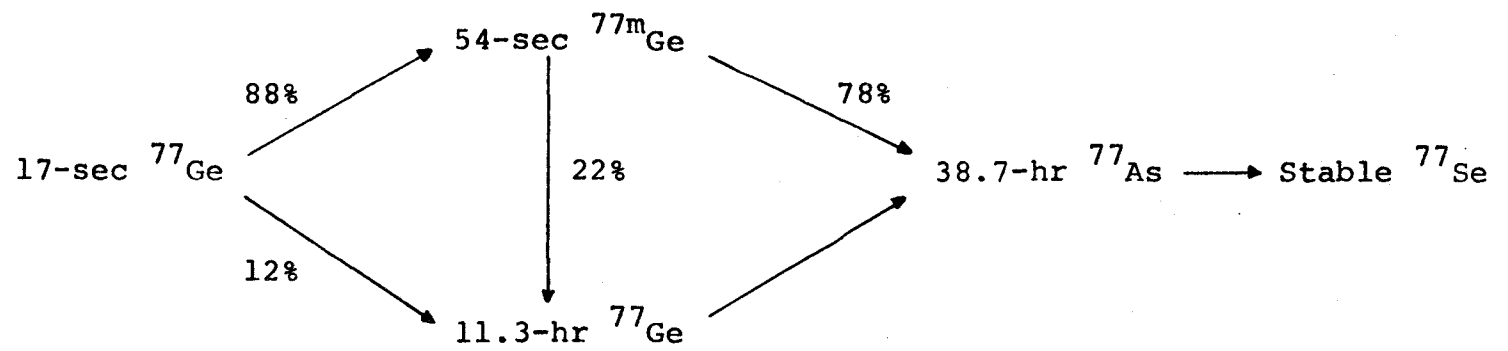
Fig. 6.   Branching Scheme of the A = 77 Mass Chain.

are 211.0, 215.6 and 264.6 keV with relative intensities of 50, 48 and 100 respectively [67].

The 21-hr ^{112}Pd decays to the ground state of 3.2-hr ^{112}Ag which in turn emits gamma-rays with energies of 618.8 keV (100), 606.1 keV (8), 691.5 keV (1.1) and 694.2 keV (6.8) [66]. The yield of ^{112}Pd was reported to be 0.12% in the thermal fission of ^{239}Pu [29].

The yield of another symmetric fission product, ^{115}Cd, is 3.8X10^{-2}% [29]. The half-life of this isotope is 53.5-hr and decays to ^{115m}In and ^{115}In emitting gamma-rays of 492.1 keV (10) and 527.7 keV (26). A gamma-ray of 336.2 keV is associated with the isomeric transition of ^{115m}In.

Of the heavy nuclides from very asymmetric fission , the A = 166 mass chain seems to be the only one suitable for this study. The yield of ^{166}Dy according to Katcoff [29] is 6.8X10^{-5}%. Because of the close similarity of dysprosium and yttrium in chemical properties, radiochemical separation of ^{166}Dy from high-yield yttrium isotopes and other rare earth fission products presents a major problem. From a consideration of the half-lives and the decay schemes of the 81.5-hr ^{166}Dy and the 26.9-hr daughter (^{166}Ho), it was decided to isolate ^{166}Ho instead of ^{166}Dy, after a state of transient equilibrium has been reached. Approximately 50% of the ^{166}Ho decays with the emission of an 80.6 keV gamma-ray.

B. ^{239}Pu Sample Preparation and Irradiation

In each experiment, two samples of ^{239}Pu were irradiated

simultaneously in the core of the McMaster swimming-pool reactor, one with either samarium or cadmium shielding, and the other one without shieldings. The simultaneous irradiations eliminate any necessity for saturation factor correction. The shieldings served to accentuate fissions in the resonance region while minimizing thermal neutron fission. Both types of shielding cut off thermal neutron effectively but the cut off energy is lower for samarium (~0.2eV) than for cadmium (~0.5eV). Radiochemical studies using monoenergetic neutrons for the very low yield fission products such as ^{72}Zn and ^{166}Dy -^{166}Ho would not be feasible because of the low neutron flux available through a monochromator.

The samarium shielding used was a solid cylinder made of commercial cement to which 35% Sm_2O_3 by weight had been added and mixed uniformly. The Sm-cement cylinder consisted of two parts, the bottom part was cast in an ordinary aluminum can used as the reactor irradiation container. The size of the Sm-cement cylinder was 2 cm in diameter, 4 cm in height, with a hole at the centre to which a sealed quartz capillary (2 mm in diameter, 1 cm in length) containing the plutonium sample could fit in. The upper part acted like a plug, 2 cm in diameter and 1 cm in height. It was calculated that the sample in centre position was being shielded by 1.8×10^{21} atoms of Sm/cm^2. However, the shielding made in this way is expected to be less effective compared to that made from pure samarium metal as used by Regier etal. [46], because of the perturbation effect of the Sm-cement on the neutron flux, and

"windows" in the Sm-cement as a result of imperfection in packing.

Cadmium sheet of 1 mm in thickness was used to wrap around the sealed quartz capsule which contained the plutonium sample for shielding purposes. The effective shielding was calculated to be 4.6×10^{21} atoms of Cd/cm^2.

The samples were PuAl-alloy containing 13.9% plutonium (96.1% ^{239}Pu). Typically the amount of ^{239}Pu in the unshielded sample was ~0.1mg and 10 and 20 times more respectively for the samarium and cadmium shielded ones. Before sealing into the quartz tube, the PuAl-alloy was wrapped in 0.001" thick aluminum foil serving as recoil fission-product catcher.

The positions in the reactor core for the shielded and non-shielded samples were chosen in such a way that the total number of fission events in both samples were not very different, usually in the order of 10^{13} to 10^{14}. The thermal neutron fluxes were 2.0×10^{13} and 1.4×10^{13} n/cm^2-sec respectively for the shielded and nonshielded samples.

Cadmium ratios for both manganese and gold of these positions were measured as follows. Cadmium cylinders 1 cm in diameter and 3 cm in height with wall thickness of 0.8mm were used. The samples of manganese and gold were in solution form (12 mg/ml for Mn and 5.6 mg/ml for Au) so that self-shielding correction can be avoided. They were sealed in small quartz capillaries for irradiations. The cadmium ratios were determined by counting the

^{56}Mn (846.9 keV) and ^{198}Au (411.8 keV) activities using a
40-cm^3 Ge(Li) detector system, and then comparing the count rates
of the non-shielded and the Cd-shielded samples after necessary
corrections of sample weights and decay factors.

The contribution of fast neutron induced fission in the
shielded samples was estimated in one run by irradiating a known
amount of metallic ^{232}Th in similar shielding and in the same
position, soon after the completion of the irradiation of the
shielded ^{239}Pu sample. Fission product gamma-ray spectra for
^{232}Th (n,f) were recorded with the Ge(Li) counter and compared with
the gross fission product gamma-ray spectrum obtained for the
shielded ^{239}Pu sample under similar conditions. Since ^{232}Th
fission can be caused by fast neutrons only, the contribution of
fission by fast neutrons in the ^{239}Pu sample can be estimated from
the comparison.

In the studies of ^{72}Zn, ^{112}Pd and ^{115}Cd, only thermal and
epi-Sm fission measurements were made. The samples prepared in
the way as described above, were irradiated for six hours in one
run and four hours in the other. Both were cooled for ~24 hours
before carrying out the radiochemistry. The total number of fission
events in the samples were ~10^{13}.

For ^{77}Ge, both thermal to epi-Cd and thermal to epi-Sm
fissions were studied. The samples were irradiated for 2 hours in
the case for epi-Sm and 4 hours for epi-Cd experiments; both were
cooled for ~12 hours. A total of ~10^{13} fissions occured in each

sample.

For ^{77}As, the samples were irradiated for 4 hours and cooled for 36 hours. Only thermal and epi-Cd fissions were studied.

Since the yield of the A = 166 chain is very low, the samples were required to be irradiated for 20 hours to obtain ~2X10^{14} fission events in each. A cooling period of ~100 hours was necessary because of the high level of radiation of the 47-hr ^{153}Sm produced in the samarium shielding during the irradiation.

C. Ge(Li) Gamma-ray Spectroscopy

High resolution Ge(Li) detectors developed since the mid-nineteen sixties have not only been very useful in studying the fission energetics but also relieved some unnecessary and tedious radiochemistry in fission mass-yield and fragment range measurements [64], [68]. For a number of the high-yield fission products, prominent gamma rays of specific isotopes have been found to be well resolved in the gamma-ray spectrum recorded with an ordinary Ge(Li) counter [64], without any radiochemical treatment. Hence, relative yields of the high-yield fission products of any fission can be directly obtained by comparing with the Ge(Li) spectrum of the gross fission products, usually of the thermal neutron fission of ^{235}U, for which the mass-yield distribution is well-known. This technique has been employed in this work to study fluctuations in the relative yields of the asymmetric products in the epi-Cd and epi-Sm fissions of ^{239}Pu as compared with the thermal fission.

After the irradiation and an appropriate period of cooling, the quartz-sealed samples were washed with aqua regia and distilled water. The quartz capsules were then crushed open and the samples including the aluminum catcher foil were transferred to small glass vials. The epi-thermal and thermal neutron-irradiated samples were each counted twice in identical geometry at a distance of about 1 m. away from the Ge(Li) detector. The detecting system includes a 12-cm^3 co-axial Ge(Li) detector and a 40-cm^3 Nuclear Diodes circular closed-end co-axial Ge(Li) detector, coupled through an Ortec FET preamplifier and an ORTEC-435 amplifier to a Nuclear Data, Series 2200, 1024 channel analyser. The system resolution for both detectors was 4.5 keV FWHM at 1.33 MeV. Each counting was set at 1000 sec live-time and the timing was controlled by feeding pulses from a pulser during the measurement. No discrepencies were found for the live timer and the results from the pulser. The dead time of the analyzer never exceeded 10%.

D. Radiochemistry

1. Carrier solution preparations

In all the radiochemical procedures to be described, a known amount of the carrier elements of the isotopes of interest were added when dissolving the sample. The percentage of recovery was determined after completion of the radiochemical treatment. Exchange between carrier ions and the radioisotopes of the same element was ensured, and the percentage chemical yield of the

element should represent the percentage of recovery of the radioactive isotope.

For the experiments on ^{72}Zn, ^{112}Pd and ^{115}Cd, a mixed carrier solution of zinc, palladium and cadmium was prepared by dissolving the metals (analytical grade) of these elements in dilute HCl and a little of HNO_3. The concentrations of the carriers were 7.96mg for Zn, 7.77mg for Pd and 15.75mg for Cd in a gramme of carrier solution.

The germanium carrier solution ~10mg/ml was prepared by dissolving ~0.5gm germanium metal (99.9%) in 30 ml of 3% H_2O_2 and dilute HCl. This metal dissolves very slowly, and the residue was filtered and the solution made up to 50 ml.

A carrier solution of As(III) of ~10mg/ml was prepared in the following way. Approximately 1.3gm of dried analytical grade As_2O_3 (99.9%) was dissolved with 20ml of 2M NaOH, and 20 ml distilled water was added. This was neutralized with 20 ml 2M HCl and diluted to 100ml.

The carrier solution of holmium was prepared by dissolving ~0.6gm holmium metal in dilute HCl and diluted to 50 ml.

Since these experiments measured the mass-yield ratios of two samples (thermal and epi-thermal), one only needs to know the relative chemical yields rather than the absolute yields. Therefore, the knowledge of the exact concentration of the carrier solution is of no importance.

2. Sample dissolution and the removal of ^{239}Pu

The ^{239}Pu is a highly hazardous isotope because of its
4.5Mev α^- activity ($t_{1/2}$ = 20,000 years). Hence, it is desirable
to remove this element completely from the fission products as
early as possible before any further radiochemical treatments of
the samples.

Anion exchange chromatography has been very frequently
used in removing plutonium from the gross fission products. Table
3 shows the behavior of plutonium in different oxidation states in
HCl solution on a strong base anion exchange resin in the chloride
form. Plutonium (IV) in nitric acid solution is also adsorbed on
strong base anion exchange resin in the nitrate form [70]. The
distribution coefficients of Pu(IV) as a function of the concentration
on HNO_3 is shown in Fig. 7.

It is essential to have the right oxidation states for
adsorption or elution of plutonium from an anion exchange column.
The +III and +IV states are the stable and most common forms of
plutonium. Oxidizing agents such as HNO_3, $NaNO_2$ (NH_4NO_2), $FeCl_3$
etc. are able to keep plutonium in the +IV state and prevent its
reduction. On the other hand, in order to prevent the uptake of
plutonium or to achieve rapid elution one can add HI, NH_4I, SO_2
or ascorbic acid[71].

In the experiments for ^{72}Zn, ^{112}Pd and ^{115}Cd, the samples
after the Ge(Li) gross fission product gamma-ray countings were

TABLE 3

Distribution Coefficients of Plutonium on
Strong Base Anion Exchange Resin in HCl[69]

HCl Concentration (N)	1	2	4	6	8	10	12
Pu(III)			no adsorption				
Pu(IV)	1	<1	<1	30	$>10^3$	$>10^3$	$>10^3$
Pu(VI)			strongly adsorbed from HCl >6N				
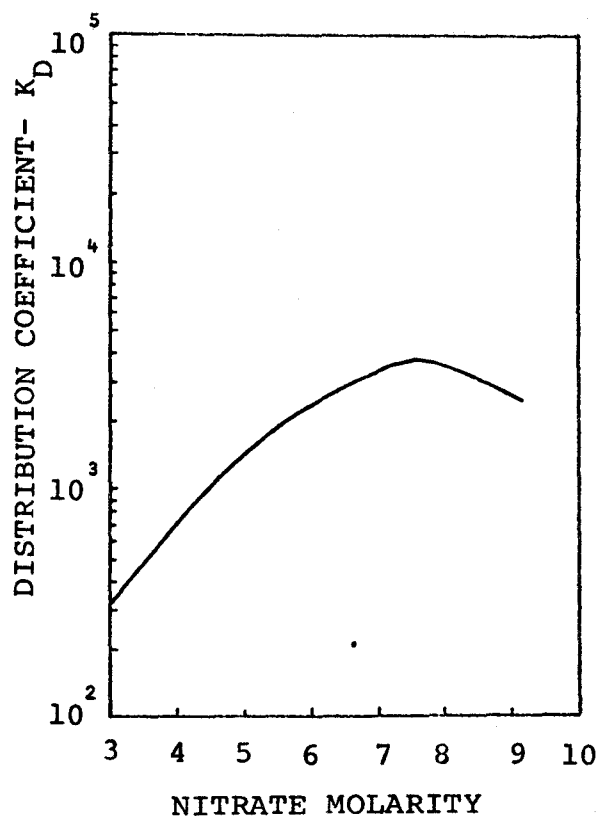
Fig. 7. Distribution coefficient of Pu(IV) on
Dowex-1X4 (50-100 mesh) from nitric acid [70].

dissolved in 2 ml of concentrated HCl and few drops of concentrated

HNO_3 in the presence of 1.5gm of mixed carrier containing ~12mg Zn^{2+},

12mg Pd^{2+} and 20mg Cd^{2+}. The sample was diluted to 2M in HCl and

passed through an anion exchange column of Dowex AG1X10, 200-400 mesh,

0.6cmX6cm in size and preconditioned with 2M HCl. All three elements

were retained on the column while ^{239}Pu in either the +III or the

+IV state simply passed through [69] and was completely removed by

washing the column with ~20ml 2M HCl.

In the experiments for ^{77}Ge, preremoval of ^{239}Pu was not

required. The samples were put into 250ml distillation flasks with

associated closed-distillation systems and dissolved by adding 1.00ml

of Ge-carrier solution and 10ml of 4M HCl saturated with Cl_2, and

then adjusted to 8M in HCl. Germanium was distilled over in a

stream of Cl_2 while ^{239}Pu was kept behind in the distillation flask.

For ^{77}As, a similar distillation procedure was used to

leave the ^{239}Pu behind.

For ^{166}Ho, the samples were dissolved in dilute HCl

and in the presence of ~12mg Ho^{3+} carrier and a few drops of

concentrated HNO_3. The solution was then brought to dryness, taken

up with 2ml of 8M HNO_3, evaporated to dryness again and finally

taken up with 2 ml 8M HNO_3. These steps assured that the plutonium

would be in the +IV state and in the nitrate form. This solution

was then passed through a Dowex AG1X10, 100-200 mesh, 0.6cmX6cm

anion exchange column which had been preconditioned with sufficient

8M HNO_3. The Pu(IV) was very strongly adsorbed on the column while

holmium went through.

3. Separation and purification of ^{72}Zn, ^{112}Pd and ^{115}Cd

The group of ^{72}Zn, ^{112}Pd and ^{115}Cd with their carriers were adsorbed on the Dowex 1X10 anion exchange column with ^{239}Pu removed. Zinc and cadmium were then eluted off with 25ml of distilled water. After scavenging twice with ferric hydroxide and once with palladium sulfide from a 2M HCl solution, the two elements were precipitated simultanously as sulfides. They were dissolved in 2M HCl and adsorbed on a column of Dowex AG2X8, 100-200 mesh, 0.6cmX16cm in size. After washing with 2M HCl, zinc was stripped of with 20ml of 0.05M HCl. The eluant was scavenged once more by ferric hydroxide precipitation. Finally, 0.5gm NH_4Cl was added to the zinc filtrate of ~20ml, the pH adjusted to ~6 using methyl red and bromthymolblue mixed indicator. The zinc was then precipitated as $ZnNH_4PO_4$ from the hot solution with 3ml of 10% NH_4HPO_4 solution. The precipitate after digestion for ~20min on a hot plate, was filtered with a 20ml-chimney and sintered-glass filtering system onto a 3cm-glass fibre filter pad. The precipitate was dried in the oven at ~110°C for half an hour and weighed for chemical yield determination.

The cadmium remaining on the Dowex AG2X8 column was eluted with 60ml of distilled water and then prepared for weighing and counting as $CdNH_4PO_4 \cdot H_2O$ in a similar way as for zinc.

Palladium was eluted from the first anion-exchange column with 1M NH_4OH after the elution of Zn and Cd. It was

further purified by ferric hydroxide scavenging, sulfide precipitation, dissolution in nitric acid and finally scavenged with silver chloride precipitation. The filtrate of palladium was then adjusted to 0.4M in HCl and ~5ml of 10% dimethylglyoximate solution was added. The precipitate of palladium dimethylglyoximate was filtered onto the glass fibre filter pad, washed with 50% ethanol, dried at ~110°C for ~20 min and finally weighed as PdDMG.

The chemical yields of Zn, Cd and Pd were approximately 80, 70 and 90%.

The zinc samples were counted several times for 50min each using a 7.5cmX7.5cm NaI(Tl) detector in connection with a Victorean preamplifier and DD2-amplifier and a Nuclear Data 256 channel analyser. The cadmium and palladium samples were counted using the 12cm^3 Ge(Li) unit described before. The cadmium samples were measured soon after their preparation and also after an appropriate growing-in period for its daughter, ^{115m}In. For palladium samples (^{112}Pd), countings were carried out via its daughter silver isotope (^{112}Ag) after a growing-in time of about 20 hours.

These radiochemical procedures were based on references (72), (73) and (74).

4. Separation of ^{77}Ge

Simple radiochemistry for the separation of ^{77}Ge was possible with a fairly high decontamination factor by specific distillation of GeCl$_4$[75]. The samples were dissolved in the way as described in section (2-C-2) in a closed distillation system.

The solution was ~20ml in volume and 8M HCl. Germanium was distilled off in a stream of Cl_2 gas at temperature kept below 110^oC. Five ml of the distillate was collected in 5 ml of distilled water cooled in an ice bath. Chlorine in the distillate was expelled by passing air through it, and then the solution was adjusted to 6M in HCl and cooled in ice. Germanium sulfide was precipitated in the presence of a few mg of KI, centrifuged and washed with 6M H_2SO_4 presaturated with H_2S. The precipitate was filtered onto a glass fibre filter pad in the usual way, dried at 110^oC and weighed as GeS_2. The chemical yield ratio was further checked by an activation method after all ^{77}Ge had virtually decayed. The chemical yields were about 95%.

The samples were counted with the $40cm^3$ Ge(Li) detector system. The spectra recorded (to be shown in the next section) revealed the presence of ^{132}Te, ^{132}I and ^{135}Xe, the latter had grown in from ^{135}I. However the decontamination was sufficient for ^{77}Ge activity determination using the prominent 254keV gamma-ray and the 211-215 keV doublet. The energies of the gamma-rays and the half-life calibrations both confirmed that they were free of interference from other gamma transitions.

Since ^{77}Ge may also be produced by stable ^{76}Ge through $^{76}Ge(n,\gamma)$, the aluminum foil used for wrapping and as a recoil catcher for the samples were also investigated for possible germanium content. As a result, no detectable quantity of germanium was found.

5. Separation and purification of ^{77}As

There are two common methods of isolating arsenic activities from fission products [75], namely the solvent extraction of As(III) as iodide with $CHCl_3$, and the distillation of As(III) from a hydrochloric acid solution. Since the yield of arsenic activities are relatively low, the solvent extraction or the distillation procedure usually has to be carried out repeatedly to obtain a radiochemically pure sample. Not only is the procedure tedius but it also frequently ends up with low chemical yields.

In the present work, it was found in preliminary experiments that only one cycle of the distillation and further purification with an anion exchange column and sulfide precipitation would give a reasonably clean arsenic sample of fairly high yield.

The plutonium samples were dissolved in 50ml distillation flasks by adding 2ml of As^{3+} carrier solution (~13mg As^{3+}) and a few mg each germanium carrier and tellurium hold-back carrier, and 6ml of 9M HCl, in the presence of Cl_2 gas. The ^{77}Ge - ^{77}As separation was properly achieved by distilling ^{77}Ge off both samples side by side within 20min in a stream of Cl_2 gas. The volume of distillate collected was ~4ml. Since ^{77}As and its carrier would be in the +V state under such conditions, it remained in the solution[75].

The Cl_2 in solution was then expelled by passing nitrogen through. A suspension of 0.3ml hydrazine hydrate and 13ml of concentrated HCl were added into the distillation flask together with 0.25 gm of boric acid dissolved in 7ml of conc HCl. Twenty milliliters of the solution was then distilled off using nitrogen

as a carrier gas and the distillate was collected in 10ml of ice-cooled water. After adding another 20ml of conc.HCl into the distillation flask a further 20 ml of distillate was collected. The arsenic in the +III state was distilled over.

The distillate was then diluted to 4M in HCl and passed through an anion exchange column of Dowex AG1X10, 100-200 mesh, 1.0cmX10cm and preconditioned with 4M HCl. Contaminants carried over in the distillate such as ^{132}Te and the iodine isotopes were efficiently adsorbed on the column while As^{3+} passed through.

Finally the arsenic in the filtrate was precipitated with H_2S. The As_2S_3 was filtered, dried and weighed in a similar way as described for zinc. Chemical yield ratios of the thermal to epi-Cd samples were obtained and further checked by the reactivation method (by ^{75}As (n,γ) ^{76}As) after completion of radiocounting. The chemical yield was ~80%.

The samples were counted with the 40cm^3 Ge(Li) system. The gamma-ray spectra, to be presented in the next chapter, showed that a clean ^{77}As was obtained.

It is interesting to note that if no tellurium(IV) was added to the solution in the distillation flask as a hold-back carrier, the minor amount of ^{132}Te carried through was impossible to remove by the anion exchanger.

6. Separation and purification of ^{166}Ho

Rare earth elements have been frequently separated as a group as fluorides and then separated from each other on cation

exchange columns using α-hydroxy-isobutyric acid (α-HIB) as an eluant [77]. A reproducible pattern of elution in the order that rare earths with higher atomic numbers are eluted in the earlier fractions than the lighter ones can always be obtained with these elements present in the +III state. The relative distribution coefficients are shown in Table 4. Note that the position of yttrium, chemically behaving like a rare earth element, nearly completely overlaps with dysprosium and is close to holmium.

Since the differences in the distribution coefficients of adjacent heavier rare earths are very small in the cation exchange system using α-HIB as eluant, good separation could only be obtained if the pH and concentration of the eluting agent are carefully adjusted. Figure 8 clearly shows the effect of the pH on the elution positions of the elements. The choice of resin of different cross-linkages is also of relevance. While resins of higher cross-linkages give good separation for certain rare earths at increased temperature, similar separation can be achieved using resin with lower cross-linkage at room temperature. [79] The latter is often preferred because difficulties arise at higher temperatures.

At an early stage of this work an attempt was made to obtain a complete separation of dysprosium from yttrium, specifically to obtain a clean ^{166}Dy activity (with carrier) out of ~10^6 times as much carrier-free yttrium activities in the fission products. This was often possible using an anion exchange resin in the

TABLE 4

Separation Factors of Rare Earth Elements on
Dowex-50 with Ammonium α-HIB as Eluant [78]

La	34.10	Dy	0.26
Ce	16.70	HO	0.16
Pr	10.45	Er	0.13
Nd	6.60	TM	0.10
Pm	4.10	Yb	0.075
Sm	2.25	Lu	0.055
Eu	1.40	Y	0.25
Gd	1.00	Cm	3.45
Tb	0.49		
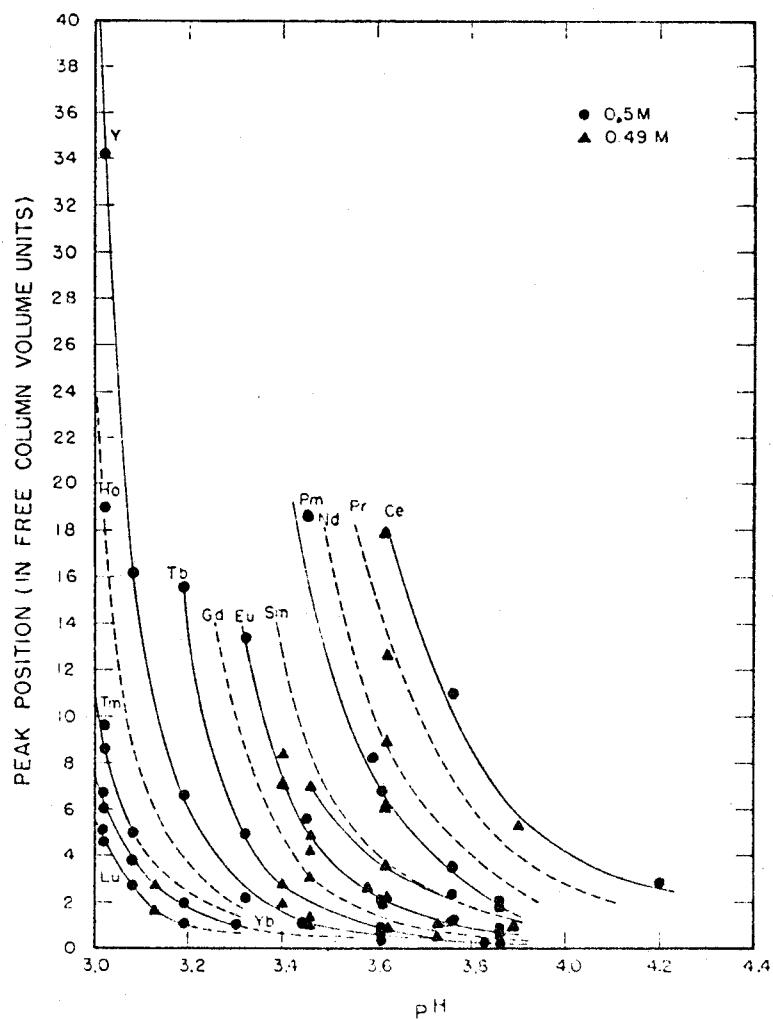
Fig. 8. Elution peak position as a function of pH for trace lanthanides from Dowex-50X4 with 0.5 M ammonium α-HIB [78].

ethylenediaminetraacetate (EDTA) form and eluting with dilute disodium-EDTA solution. Figure 9 shows the distribution coefficients of the lanthanides on the anion exchange resin in the EDTA form. Successful separation of ^{165}Dy from yttrium and other rare earths has also been reported by Alimarin et al. [81]. The resin we used was Dowex AG1X10, 200-400 mesh, 0.6cm X25cm and preconditioned with 1M ammonium acetate, H_2O and then with 0.1M Na_2-EDTA solution until free of chloride ion. Dysprosium activity with 10mg carrier which has been separated as a group of rare earths was precipitated as hydroxide, dissolved in 2MHCl, evaporated to dryness and finally taken up with 1ml of 0.005M Na_2-EDTA solution. This was transferred to the column and then eluted with 0.01M Na_2-EDTA solution at a flow rate of 1 drop/min. Yttrium was eluted before dysprosium. Radiochemically pure dysprosium free of yttrium activity was often obtained.

This attempt to isolate ^{166}Dy was dropped because of the following difficulties: First, radiochemical purity was not always reproducible. Second, the complete removal of EDTA from the dysprosium solution is essential so that the chemical yield determination would not be affected. However, this always ends up with additional loss of chemical yield. Third, since the separation scheme took about 24 hours, the equilibrium of ^{166}Dy-^{166}Ho might be affected unpredictably; and the energy of the gamma-ray of ^{166}Dy (82.5keV) is very close to that of ^{166}Ho (80.6keV), thus counting with NaI(Tl) detector may give erroneous result.

The procedure developed in this study for the separation
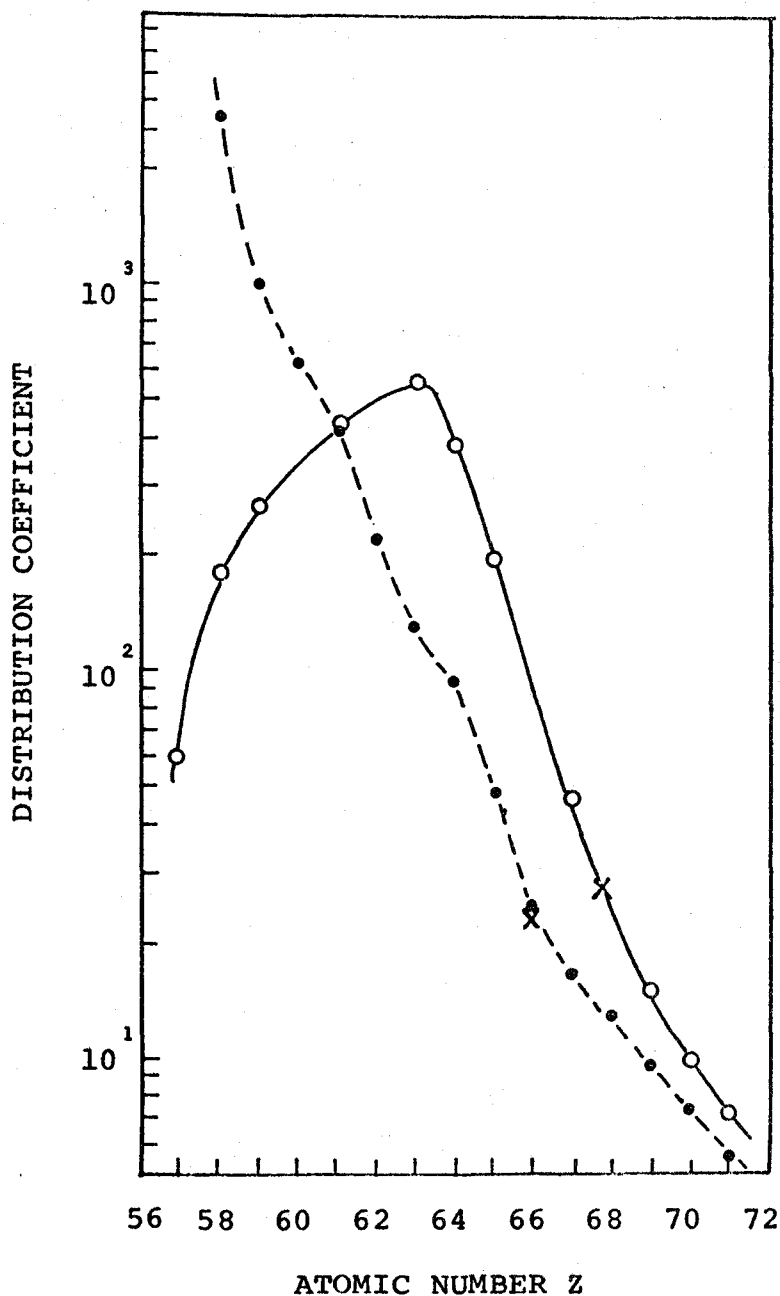
Fig. 9. —o—o—o— Distribution coefficient in the system: Amberlite IRA-400 (H_2Y^{2-}) — 0.01M Na_2H_2Y aq. (Y = EDTA). ---●---●---●--- Relative distribution coefficients (Gd taken as standard) in the system: Dowex-50X12 — α-HIB at 87°C [80]. X = yttrium.

of holmium from the rest of the rare earths and yttrium isotopes was based on reference (82). The cation exchange resin of Dowex-50X4, minus 400 mesh was treated with 6M HCl, 1M NH_4SCN, 6M HCl, H_2O, 1M NH_4OH and H_2O, in the respective order. The size of the column was 1cmX36cm, and 0.5M α-HIB of pH 3.16 was used as eluting agent. The sample which contained the rare earth activities and ~13mg of Ho^{3+} carrier was usually taken up with minimum amount (0.3ml) of the same resin and then transferred onto the column. It was then washed with 2ml of the eluting agent and then eluted under controlled pressure to adjust the flow rate to ~7ml/hour. Fig. 10 shows an elution curve obtained under the described condition in the preliminary experiment for the separation of ^{166}Ho with carrier from ^{165}Dy tracer. Fig. 11 shows a similar elution curve for the separation of stable holmium and carrier free ^{90}Y. Since complete separation was not obtained, it was necessary to discard minor portions in the overlapping region.

The detailed procedure for the isolation of ^{166}Ho from the gross fission products is given below.

The solution of the sample from which ^{239}Pu had been removed by an anion exchanger in the nitrate form was in 8M HNO_3 and contained the holmium carrier and the fission products. The $Ho(OH)_3$ was precipitated with NH_4OH and then dissolved in 2M HCl and precipitated as HoF_3 with 38% HF. The fluoride was digested on a hot bath, centrifuged and washed with 0.1M HF, and then decomposed by adding 3ml saturated hydroboric acid solution and 2ml conc HNO_3. The $Ho(OH)_3$ was precipitated again from the diluted solution, dissolved in conc HCl and passed through an anion exchange
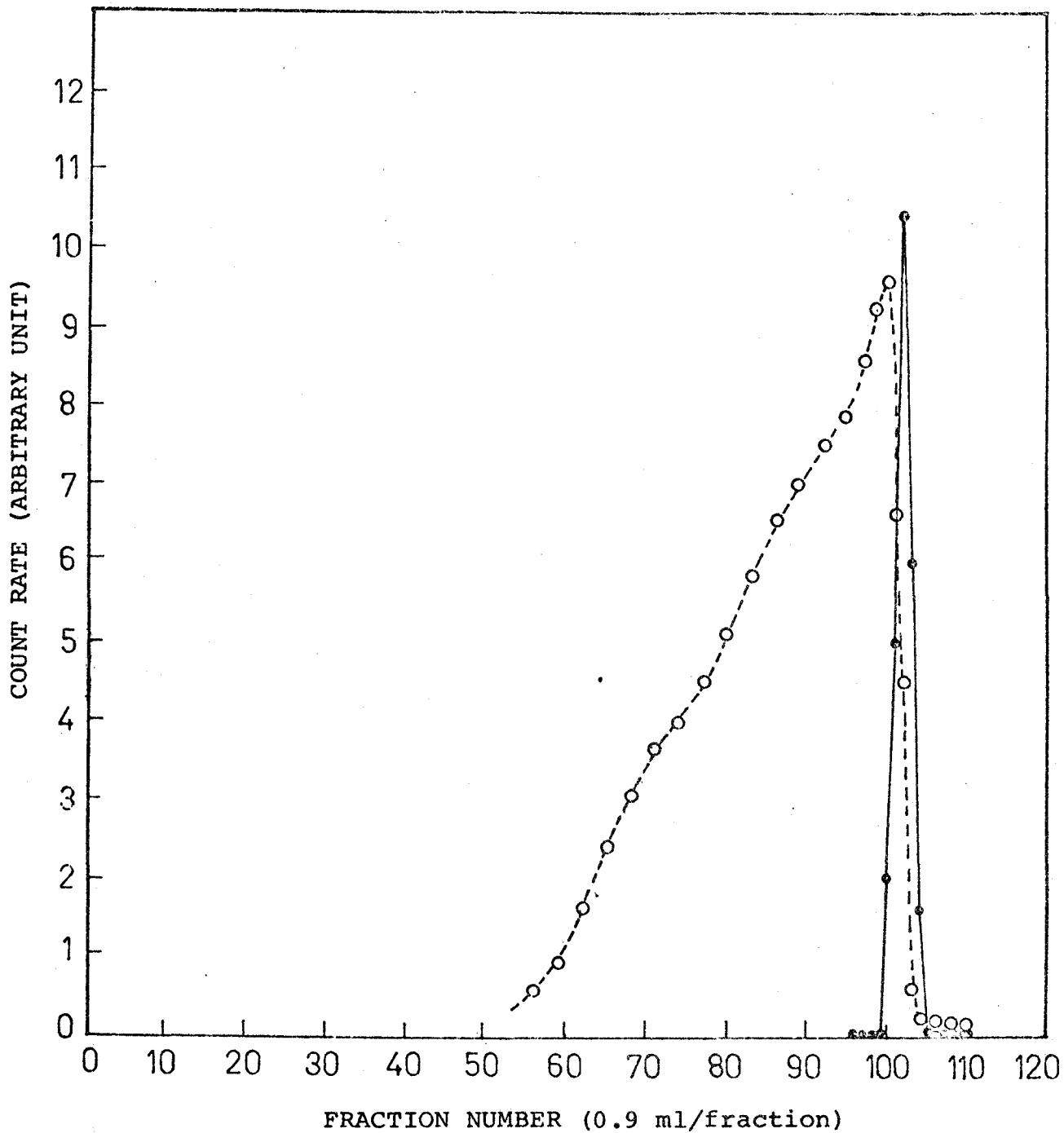
Fig. 10. Elution curve of [166]Ho + carrier (dashed line) and [165]Dy tracer (solid line) from Dowex-50X4 with 0.5M α-HIB as eluant (pH 3.16).
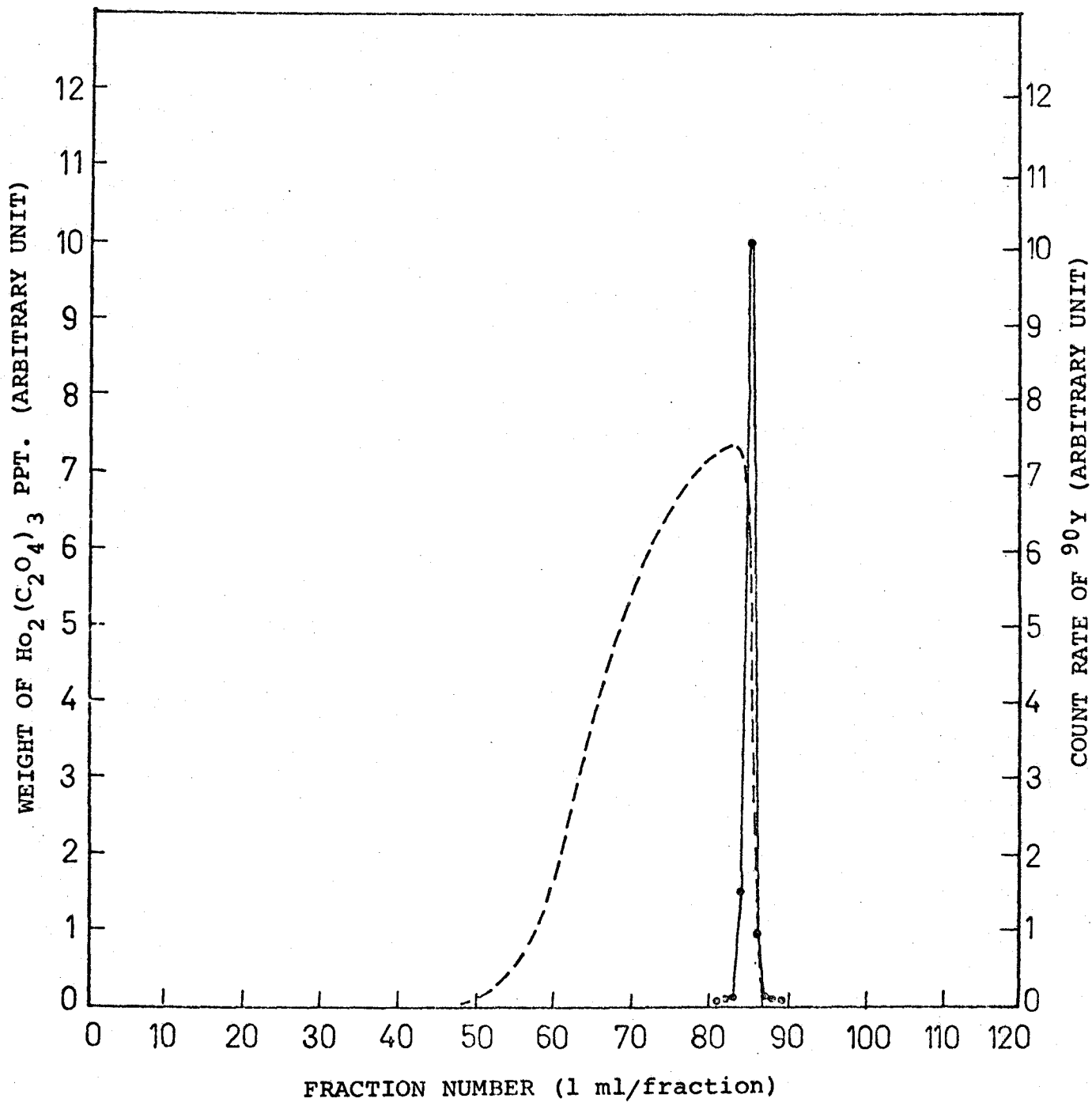
Fig. 11.   Elution curve of holmium (dashed line) and ^{90}Y (solid

line) from Dowex-50X4 with o.5M α-HIB as eluant (pH 3.16).

column of Dowex-AG1X10, 100-200 mesh, 0.6cmX6cm, preconditioned

with conc HCl. From the diluted filtrate the holmium hydroxide

was precipitated and then dissolved in 3 drops conc HNO_3 and

diluted to 30ml. About 0.3ml of wet cation exchange resin of Dowex-

50X4, minus 400 mesh was added to take up the holmium.

In the next step to separate ^{166}Ho with holmium carrier from

the rest of the rare earth fission products, the above resin was

transferred to the cation exchange column of Dowex-50X4, minus

400 mesh, 1cmX36cm, prepared as described before. The column was

eluted with 0.5M α-HIB solution of pH 3.16 at a flow rate of ~7ml/hr.

Fractions of the eluant were collected at 10min intervals and they

were examined for the presence of holmium by the addition of

saturated oxalic acid. The later fractions containing holmium

which might also contain yttrium isotopes were checked with the

NaI(Tl) detector for the 10-hr ^{93}Y activity (E_γ =267keV). Fractions

free of yttrium activity were combined and holmium oxalate completely

precipitated, digested on a hot bath, centrifuged and washed with

dilute oxalic acid. Finally the precipitate was taken up with

water and filtered onto a glass fibre filter pad, washed with water

and 50% alcohol. The samples were dried in a furnace kept at 200-

240°C for an hour, cooled and then weighed. This was repeated until

constant weight was obtained. The chemical form under such condition

is known to be $Ho_2(C_2O_4)_3 2H_2O$ [83]. Chemical yield ratio was

calculated and the actual yield was about 60%.

After the chemical yield determination, the samples were

carefully placed into the bottom of a 2cmX15cm test-tube and

2ml 6M HCl added for dissolution. It was then counted with a

7.5cmX7.5cm well-type NaI(Tl) detector coupled to the preamplifier,

amplifier and the multichannel analyser system as described before.

Each sample was counted several times for 4000sec, background

count rates were subtracted after each counting. The resulting

^{166}Ho spectra (to be shown in the next chapter) matched identically

with standard ^{166}Ho spectra. In addition, the half-life measurement

also confirmed the purity of the ^{166}Ho samples.

It has to be pointed out that at the time of the separation

of 27.2-hr ^{166}Ho from other rare fission products, any primary

formed ^{166}Ho has undergone decay of several half-lives. Therefore,

the ^{166}Ho activity was actually the daughter of 82-hr ^{166}Dy, which

represented the cumulative yield of the 166 mass chain. At the

time of the separation of ^{166}Dy - ^{166}Ho, apparently transient

equilibrium had been reached and since the two cation exchange columns

of the thermal and epi-Sm samples were running side by side, the

time difference between the two samples was negligible in the

regard of when transient equilibrium was disrupted.

It is also necessary to investigate the possible contamination

sources of the very low yield   A = 166 chain from fission of

^{239}Pu. The ^{166}Ho can be formed from the stable holmium via ^{165}Ho

(n,γ) reaction and ^{166}Dy via the double neutron capture of stable

^{164}Dy. Any contamination due to natural rare earths in the

^{239}PuAl-alloy or in the aluminum catcher foil could be discovered

from the following consideration.

The relative abundances of the rare earths in nature are

shown in Table 5. Among the heavier rare earths (> Ho), ^{174}Yb

TABLE 5

Relative Abundances of Rare Earth Elements[84]

$Si = 1X10^6$

Sc	28.0	Gd	0.684
Y	8.9	Tb	0.096
La	2.00	Dy	0.556
Ce	2.26	Ho	0.118
Pr	0.40	Er	0.316
Nd	1.44	Tm	0.032
Pm	0	Yb	0.220
Sm	0.664	Lu	0.050
Eu	1.87		

and ^{176}Lu are two isotopes with relatively high neutron capture cross-sections. The products of these isotopes from (n,γ) reactions are 4.2-d ^{175}Yb (γ -rays: 113.8 keV and 396.1 keV) and 6.8-d ^{177}Lu (γ -rays: 113.0 keV and 208.3 keV). One can therefore estimate the relative activities of ^{166}Ho, and ^{175}Yb and ^{177}Lu formed for any quantity of rare earths under similar conditions of irradiation and radiochemical treatments as for the plutonium samples. If significant amount of ^{166}Ho were produced by ^{165}Ho (n,γ) and for ^{164}Dy (2n,γ) - ^{166}Dy - ^{166}Ho reactions rather than from fission alone, both ^{175}Yb and ^{177}Lu should be detected as described below.

From the elution pattern of the rare earths from the cation exchange resin column with α-HIB$^{(78)}$,ytterbium and lutetium were expected to appear in earlier fractions than holmium in the elution. Fractions before the appearance of holmium were divided into three portions. A few mg of rare earth carrier (Eu^{3+}) was added to each portion and then saturated oxalic acid added for the precipitation of rare earth oxalate. The oxalate was counted in a similar way as for holmium oxalate. No 4.2-d ^{175}Yb (396, 114 keV) and 6.8-d ^{177}Lu (113, 208 keV) activities were detected with the 7.5cmX7.5cm well-type NaI(Tl) counter. Thus the possibility of contamination due to the presence of natural rare earths can be excluded.

CHAPTER 3

EXPERIMENTAL RESULTS

A. Treatment of Gamma-ray Spectra

The digital gamma-ray spectra recorded were usually plotted and peak positions located for energy calibration. Intensities of gamma-rays were determined by summing the count rates in each channel in the peak and subtracting a background which was estimated by manually fitting a smooth background curve through the spectrum. The count rates of fission products from thermal and epi-Cd and from thermal and epi-Sm were compared to give the corresponding mass-yield ratios after necessary decay factor correction. In cases with radiochemical treatments, chemical yield corrections were also made.

B. The Thermal to epi-Cd and the Thermal to epi-Sm Mass-Yield Ratios of Products from Asymmetric Fission

Typical gross gamma-ray spectra of the fission products of ^{239}Pu after ~20 hours and ~100 hours cooling periods are presented in Fig. 12 and Fig. 13. Energies of the prominent gamma-rays of each nuclide used for the calculation of the activity ratio are listed in Table 6. The spectra were consistent with those obtained for thermal neutron fission of ^{235}U by Gordon et al.[64] and Heath [85].
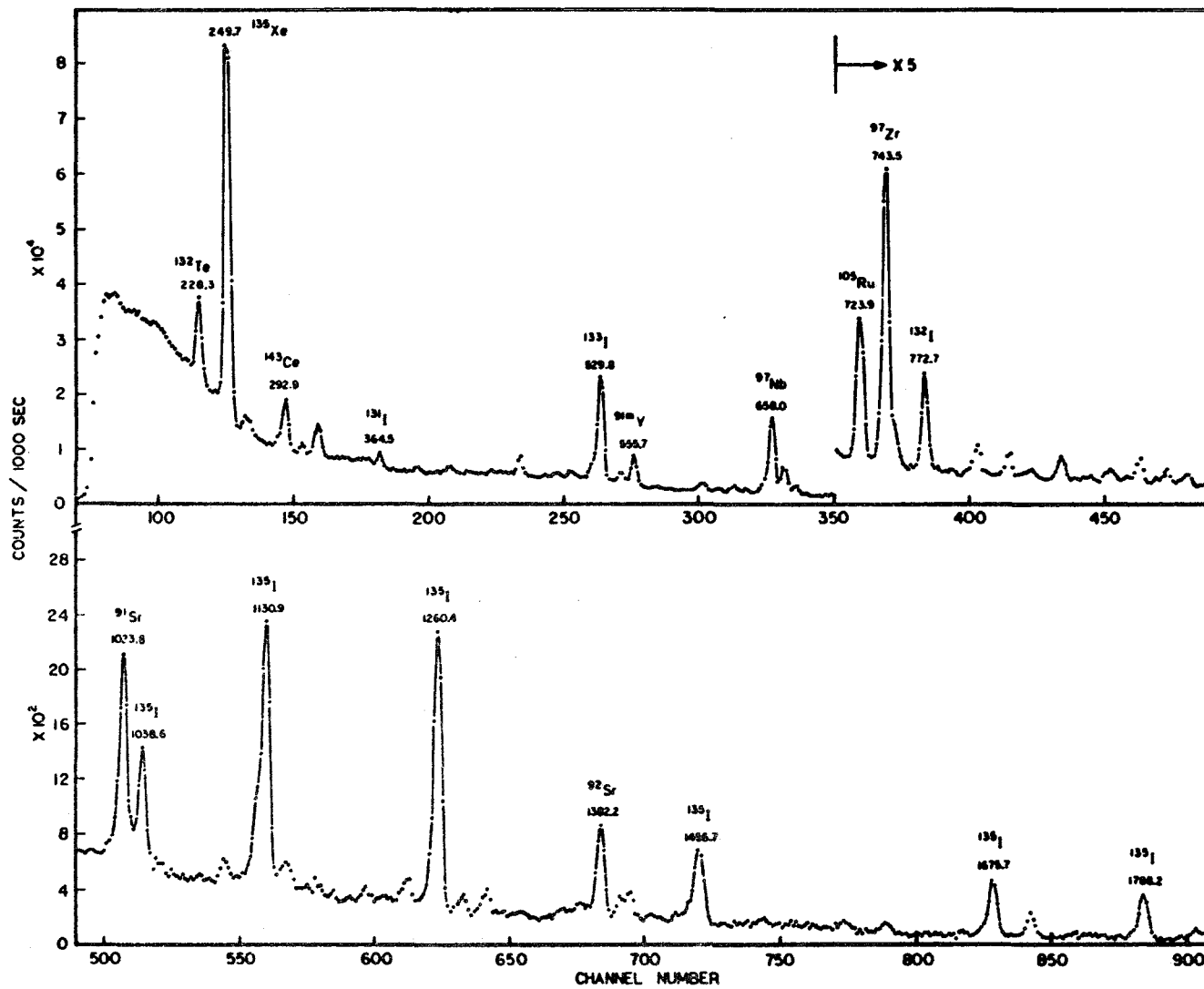
Fig. 12. Gross fission-product Ge(Li) spectrum for ^{239}Pu (n,f), 20 hours after irradiation. (Peak energies are in keV).
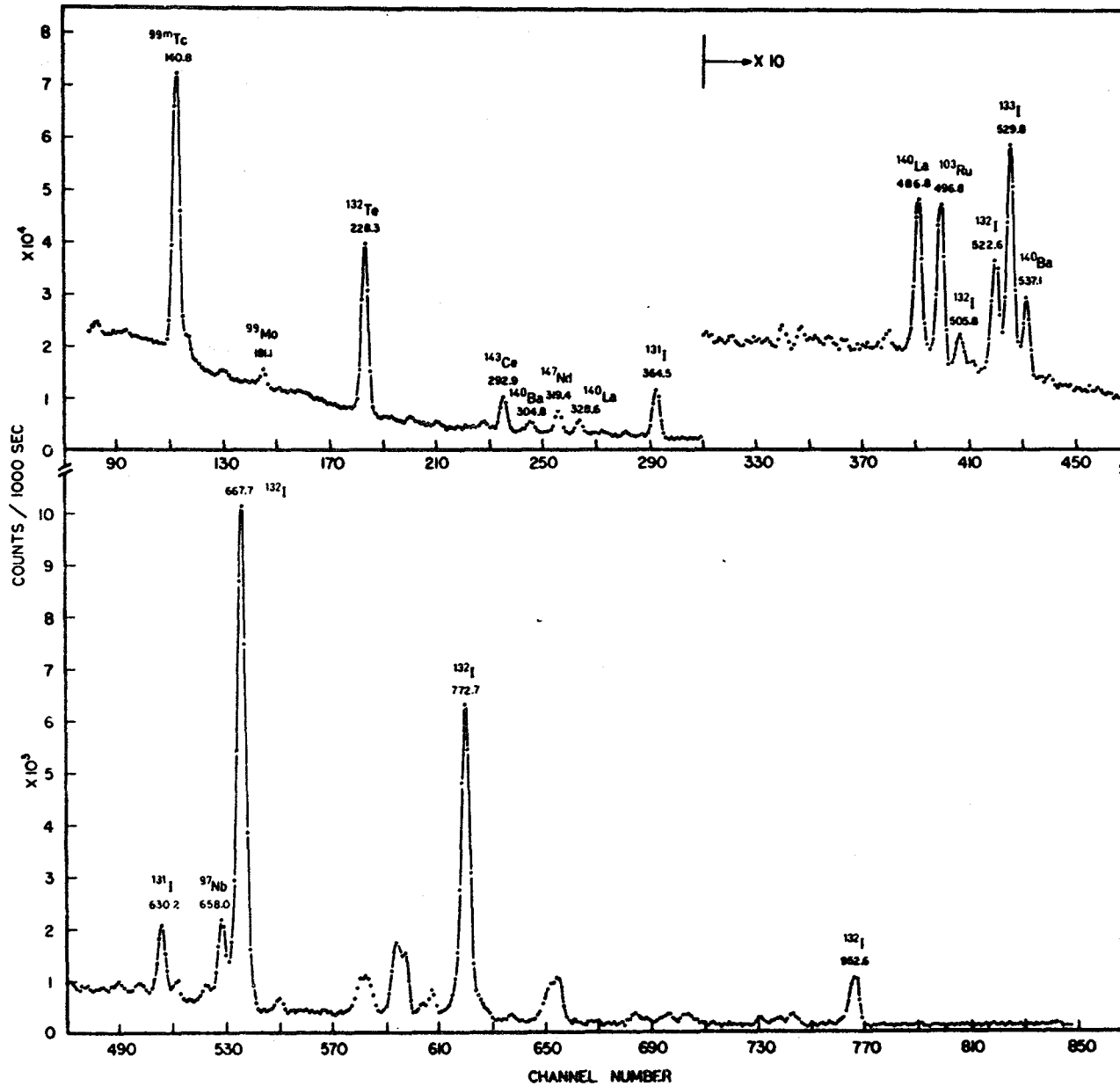
Fig. 13. Gross fission-product Ge(Li) spectrum for ^{239}Pu (n,f), 100 hours after irradiation.

TABLE 6

Prominent Gamma-rays in Gross Fission
Products Ge(Li) Spectrum

Nuclide	Half-life	Prominent γ-rays (keV)
^{85m}Kr	4.4-hr	151.2
^{91}Sr	9.7-hr	1024.3
^{91m}Y	50-min	555.6
^{92}Sr	2.7-hr	1384.0
^{97}Zr	17-hr	743.5
^{97}Nb	72-min	658.0
^{99m}Tc	6.0-hr	140.5
^{103}Ru	40-d	496.9
^{105}Ru	4.4-hr	723.9
^{131}I	8.05-d	364.5
^{132}Te	78-hr	228.3
^{132}I	2.3-hr	667.7, 772.8
^{133}I	21-hr	529.8
^{135}I	6.7-hr	1260.4
^{135}Xe	9.2-hr	249.6
^{140}Ba	12.8-d	304.8, 537.2
^{140}La	40.2-hr	328.8, 487.0
^{143}Ce	33-hr	293.3
^{147}Nd	11.1-d	319.4

Any minor components overlapping with the prominent gamma-rays were resolved. Peak areas of the prominent peaks were estimated by summing the count rates in the peak channel and subtracting a smooth background which was fitted to the spectrum. The intensities of the high-yield fission products for thermal and epi-Cd fissions, and for thermal and epi-Sm fissions, corrected for any half-life effect, were directly compared.

Table 7 shows the ratio from each run of the experiments, and the errors quoted are solely due to counting statistics. No fluctuations were observed in these activity ratios.

The thermal and epi-thermal samples were counted at identical geometry, and any sequential beta decays of the gamma transitions were allowed to go to completion or otherwise have reached the state of transient equilibrium before counting. From the mass-yield distribution curve we also see that the total yields of products from asymmetric fission virtually sum up to 200%. It is therefore possible to assume that the activity ratios represent the mass-yield ratios and hence the relative number of fission events in the thermal and epi-thermal fissions of ^{239}Pu. Thus it is implied in these data that there are no significant variations in the mass yields of asymmetric products for epi-Cd or epi-Sm as compared with thermal neutron fissions.

C. The Thermal to epi-Sm Mass-Yield Ratios of ^{72}Zn, ^{112}Pd and ^{115}Cd

Typical experimental spectra of ^{72}Zn (Obtained with

TABLE 7

Activity Ratios of Fission Products for Thermal to epi-
Thermal Fission of ^{239}Pu from Nondestructive Ge(Li) Measurements

Experiment Number	1	2	3	4	5	6	7
Activity ratio Nuclide	thermal ——— epi-Sm	thermal ——— epi-Sm	thermal ——— epi-Sm	thermal ——— epi-Cd	thermal ——— epi-Cd	thermal ——— epi-Sm	thermal ——— epi-Sm
^{85m}Kr				2.31±.06			
^{91}Sr			1.78±.07	2.38±.12			
^{91m}Y			1.72±.05	2.36±.08	1.76±.05		
^{92}Sr			1.75±.08				
^{97}Zr	2.76±.06	1.34±.02	1.73±.03	2.36±.05	1.73±.05		
^{97}Nb	2.86±.04	1.36±.02	1.75±.03	2.37±.05	1.73±.04		
^{99m}Tc	2.94±.03	1.37±.01			1.72±.02	1.23±.02	
^{103}Ru						1.22±.03	1.38±.04
^{105}Ru			1.78±.05	2.35±.06			
^{131}I					1.79±.05	1.21±.02	1.43±.02
^{132}Te	3.05±.05	1.36±.02	1.69±.04	2.31±.03	1.72±.03	1.22±.02	1.43±.02
^{132}I	2.95±.09	1.35±.03		2.37±.04	1.78±.05	1.21±.02	1.41±.02
^{133}I	2.88±.05	1.32±.02	1.73±.02	2.29±.04	1.77±.04	1.20±.03	1.39±.03

TABLE 7 (Continued)

Experiment Number	1	2	3	4	5	6	7
Nuclide							
^{135}I			1.76±.07	2.39±.12	1.75±.05	1.17±.03	1.38±.04
^{135}Xe	2.75±.02	1.34±.01	1.70±.02	2.32±.02	1.70±.03		
^{140}Ba						1.16±.04	
^{140}La						1.18±.04	1.37±.04
^{143}Ce	3.06±.09	1.28±.03	1.69±.03	2.25±.05	1.76±.04	1.19±.04	1.37±.03
^{147}Nd					1.75±.05	1.17±.04	1.38±.04
Weighted Average	2.88±.11	1.35±.03	1.73±.04	2.33±.05	1.74±.05	1.21±.03	1.40±.04
Weights of ^{239}Pu (thermal/epi-th) (mg)	0.1/0.5	0.1/1.0	0.1/0.9	0.07/1.0	0.05/1.0	0.1/1.1	0.1/1.0
Irradiation Time	6-hr	6-hr	2-hr	1-hr	4-hr	20-hr	20-hr
Cooling Time	24-hr	24-hr	12-hr	12-hr	36-hr	100-hr	124-hr

NaI(Tl) detector) and ^{112}Pd and ^{115}Cd (obtained with Ge(Li)
detector) are shown in Figs. 14, 15 and 16 respectively. Energies
of the relevant gamma peaks were calibrated as closely as possible.
Countings carried out at several intervals for each sample also
allowed to measure the half-life, and hence to determine whether
there were any interferences to these gamma-rays or not.

The count rates obtained were corrected for decay effects
and chemical yields and then compared. Results of the activity
ratios, i.e. activity of product from thermal fission of ^{239}Pu
to activity from epi-Sm fission, of the above isotopes are
presented in Table 8. Since the relative number of fission
events in the thermal and epi-Sm samples were given by the
activity ratios of the high-yield fission products as we have
shown in the last section, the thermal to epi-Sm mass-yield
ratios for these isotopes were also computed. We recall that
the definition of "R" value, discussed in Chapter 1, as measure
of the mass-yield ratios of asymmetric to symmetric fission
products as

$$R = \frac{(A_{asym}/A_{sym}) \text{ resonance}}{(A_{asym}/A_{sym}) \text{ thermal}}$$

Obviously, the mass-yield ratios we obtained for ^{72}Zn, ^{112}Pd and
^{115}Cd are actually equivalent to the "R" values.
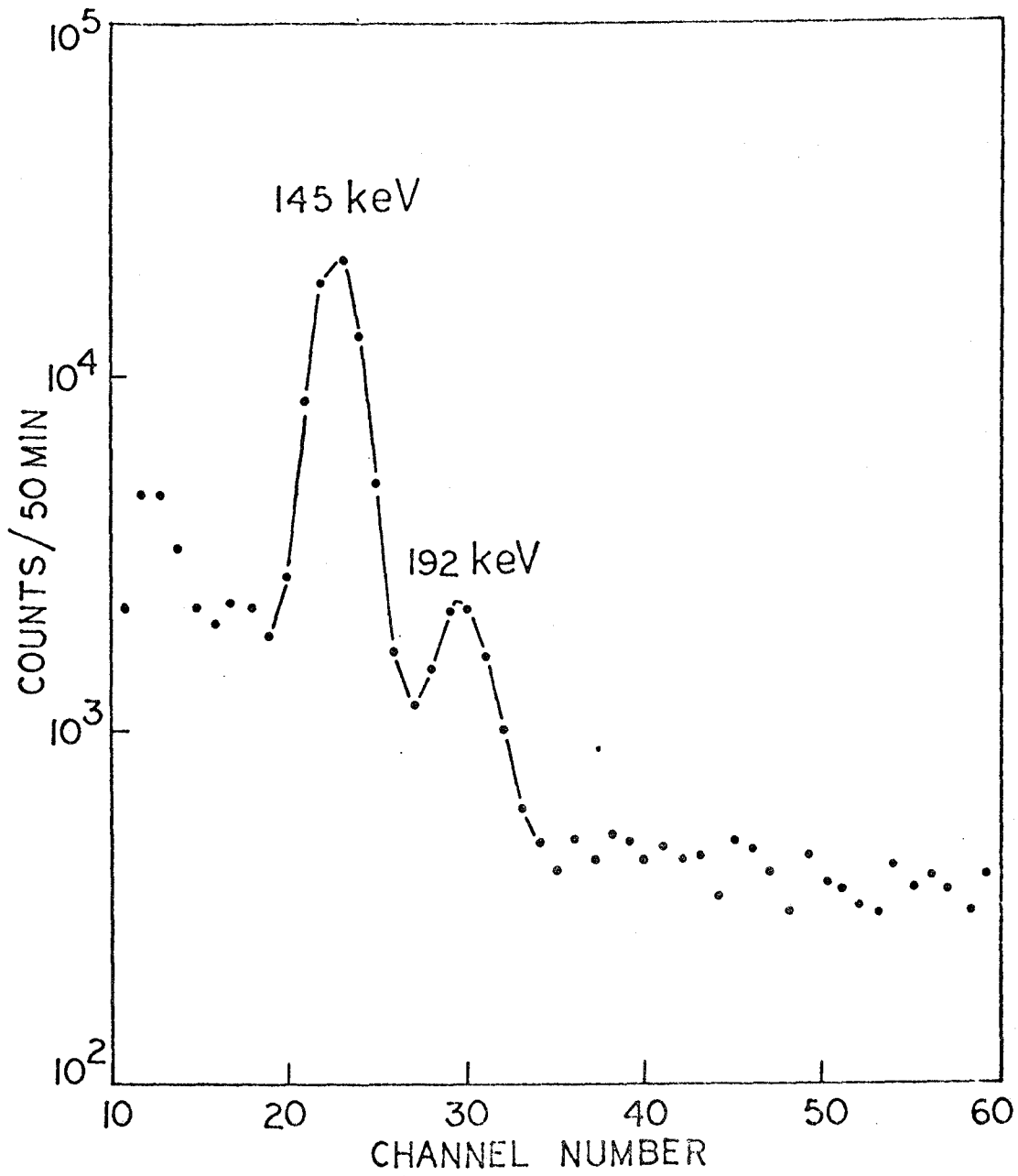
Fig. 14. NaI(Tl) gamma-ray spectrum of ^{72}Zn.
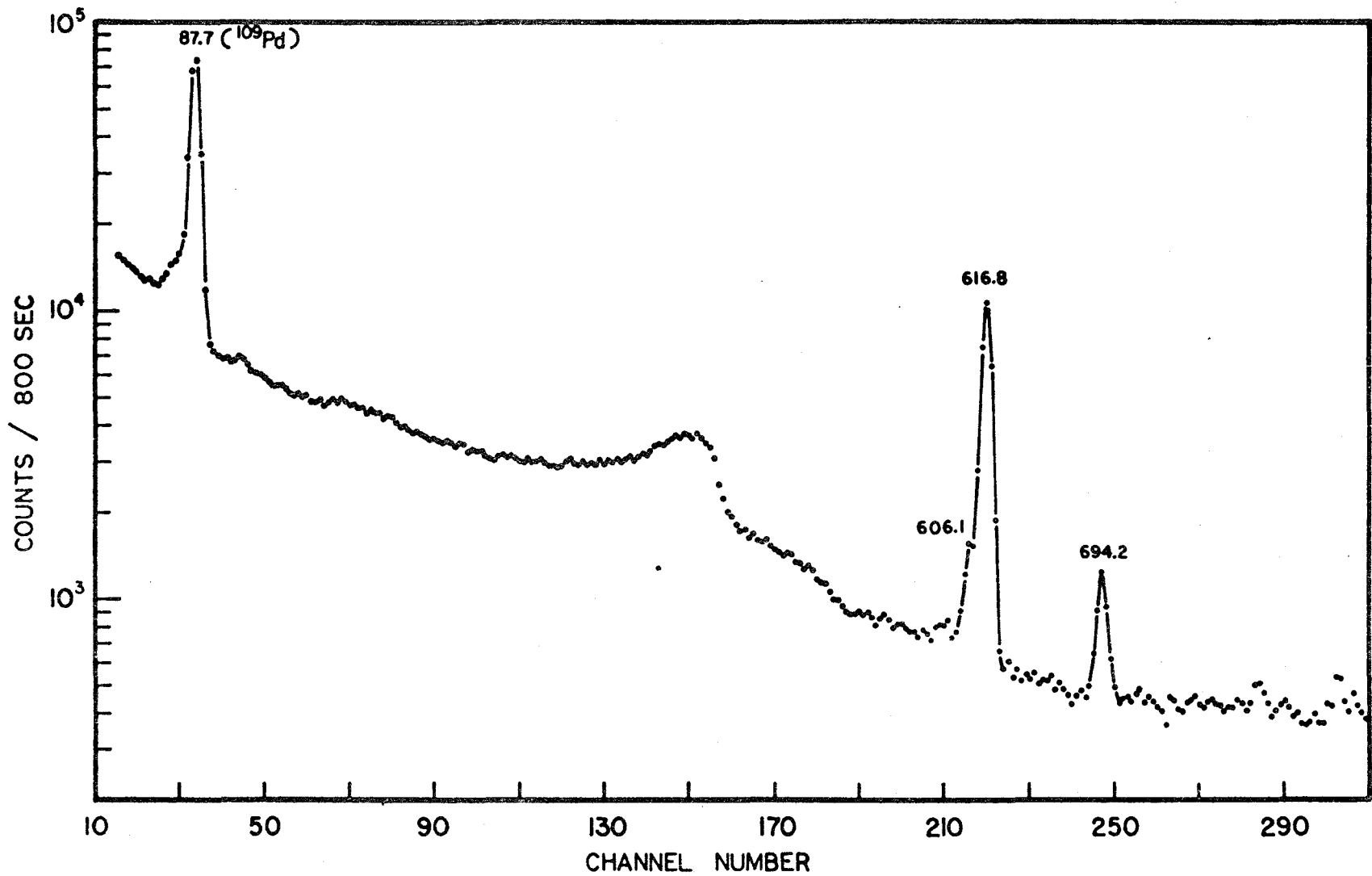
Fig. 15. The Ge(Li) gamma-ray spectrum of ^{112}Pd–^{112}Ag.
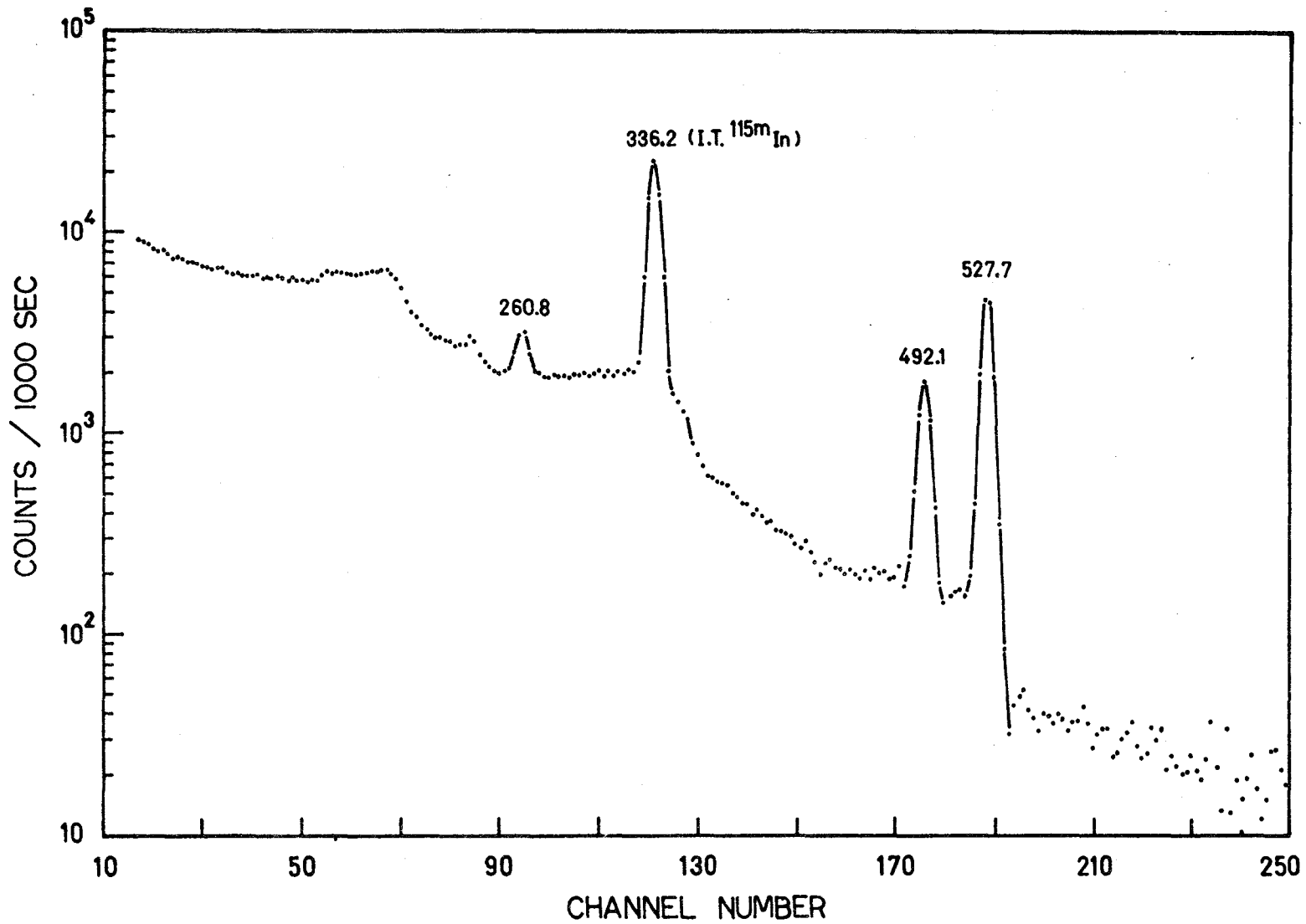
Fig. 16. The Ge(Li) gamma-ray spectrum of ^{115}Cd-^{115m}In.

TABLE 8

Measured and Normalized Mass-Yield Ratios
for Thermal to epi-Sm Fission of ^{239}Pu
(^{72}Zn, ^{112}Pd, and ^{115}Cd).

Nuclide	Measured Activity Ratio		Normalized mass-yield ratio (R)		Average % decrease
	#1	#2	#1	#2	
^{72}Zn	4.20±0.10	1.91±0.03	1.46±0.07	1.42±0.04	30±1
^{112}Pd	3.96±0.22	1.70±0.04	1.38±0.09	1.26±0.04	24±3
^{115}Cd	5.54±0.20	2.45±0.11	1.92±0.10	1.82±0.09	46±1

D. The Thermal to epi-Cd and Thermal to epi-Sm Mass-Yield
Ratios of ^{77}Ge and ^{77}As

Presented in Figs. 17 and 18 are the Ge(Li) spectra of
^{77}Ge and ^{77}As respectively. Gamma lines due to impurities are
indicated. Gamma peaks used for the activity measurements are
239.3 keV for ^{77}As, and 264.4 keV and the 211.0-215.6 keV
doublet for ^{77}Ge. Countings were usually followed through
several half-lives. Both the energy and half-life calibration
of these gamma peaks showed no interference from impurity
activities of other isotopes.

The activity ratios were computed and given in Table 9,
in a similar way as for the ^{72}Zn group. The "R" values were
also obtained.

E. The Thermal to epi-Sm Mass Yield Ratios of ^{166}Ho - ^{166}Dy

A spectrum of ^{166}Ho obtained with the 7.5cmX7.5cm
well-type NaI(Tl) detector is shown in Fig. 19 , with room background
and counter noise self-subtracted. The activity ratios and "R"
values were obtained after necessary half-life and chemical yield
corrections and presented in Table 10. These values are designated
for ^{166}Dy - ^{166}Ho because of the equilibrium of the two isotopes
at the stage of chemical separation.

F. Cadmium Ratios and Fast Neutron Fission Contribution

The measured cadmium ratios of the two in-core positions
usually employed in the irradiations of this work were in
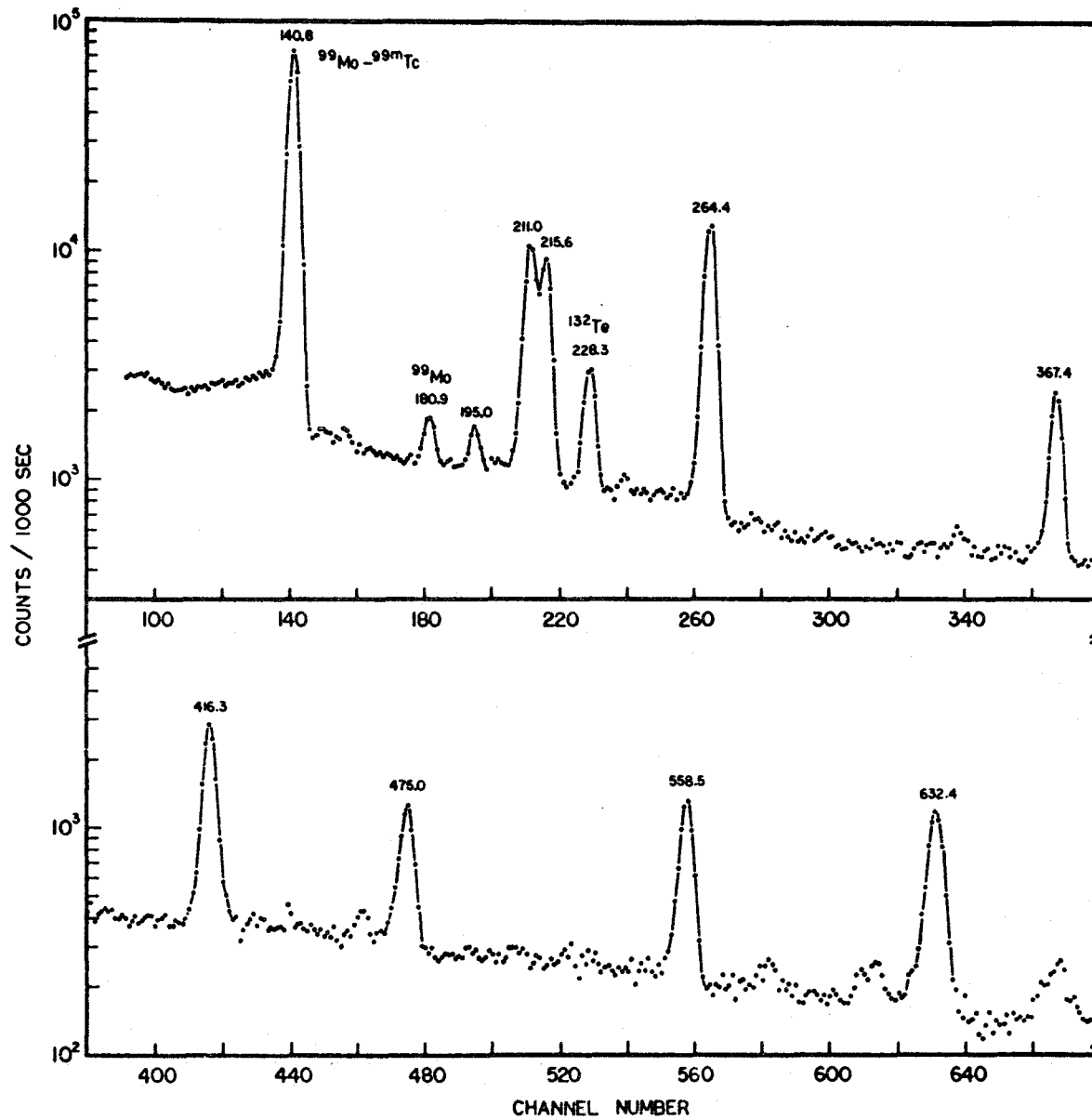
Fig. 17. The Ge(Li) gamma-ray spectrum of ^{77}Ge.
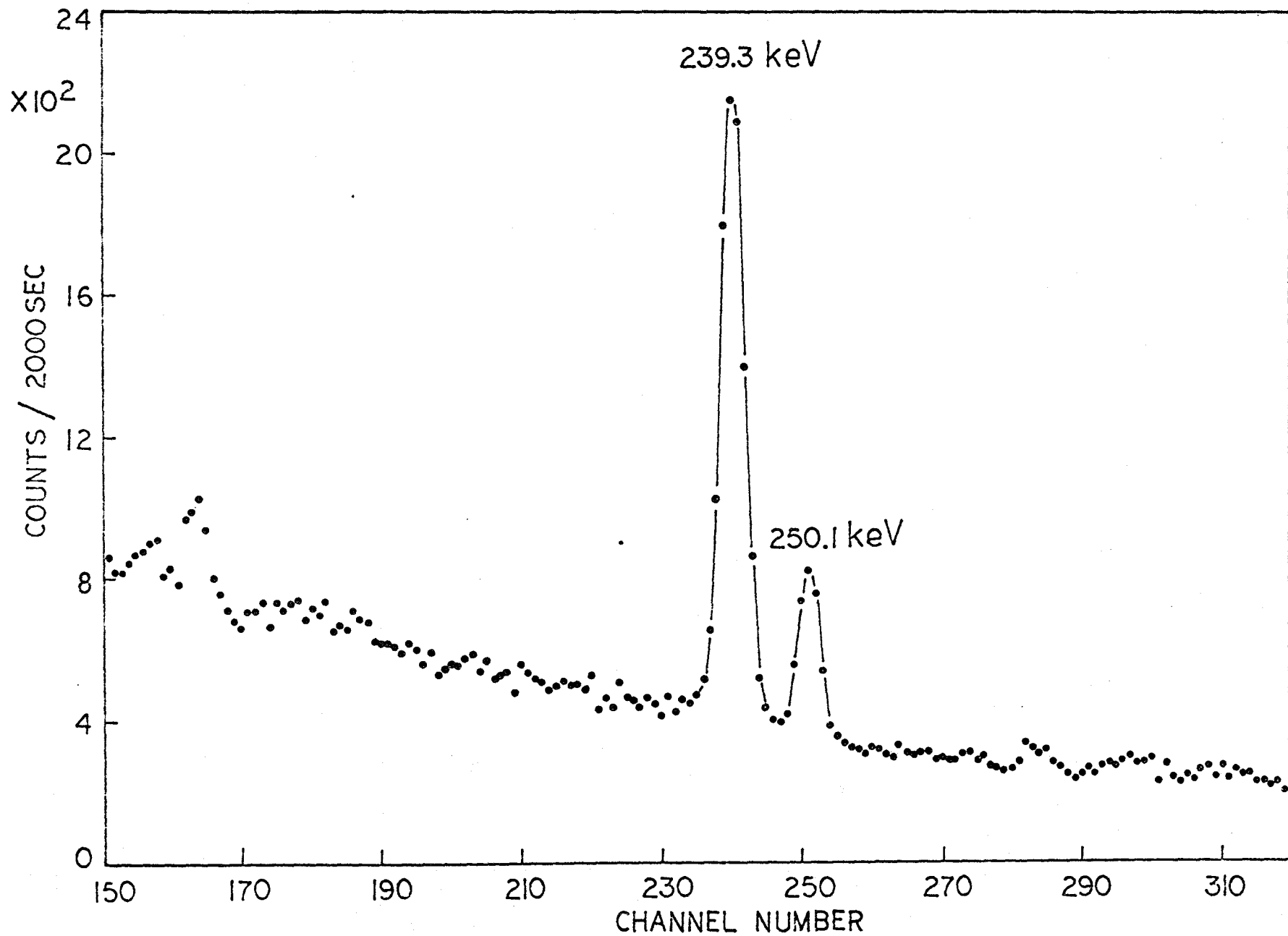
Fig. 18. The Ge(Li) gamma-ray spectrum of ^{77}As.

TABLE 9

Measured and Normalized Mass-Yield Ratios for Thermal
to Epi-thermal Fission of ^{239}Pu (^{77}Ge and ^{77}As)

| Nuclide	#3 $\frac{thermal}{epi-Sm}$	#4 $\frac{thermal}{epi-Cd}$	#5 $\frac{thermal}{epi-Cd}$	#3	#4	#5
	Measured Activity Ratio			Normalized Mass-Yield Ratio (R)		
^{77}Ge	1.87±0.08	2.50±0.10		1.08±0.05	1.07±0.05	
^{77}As			1.79±0.08			1.03±0.05
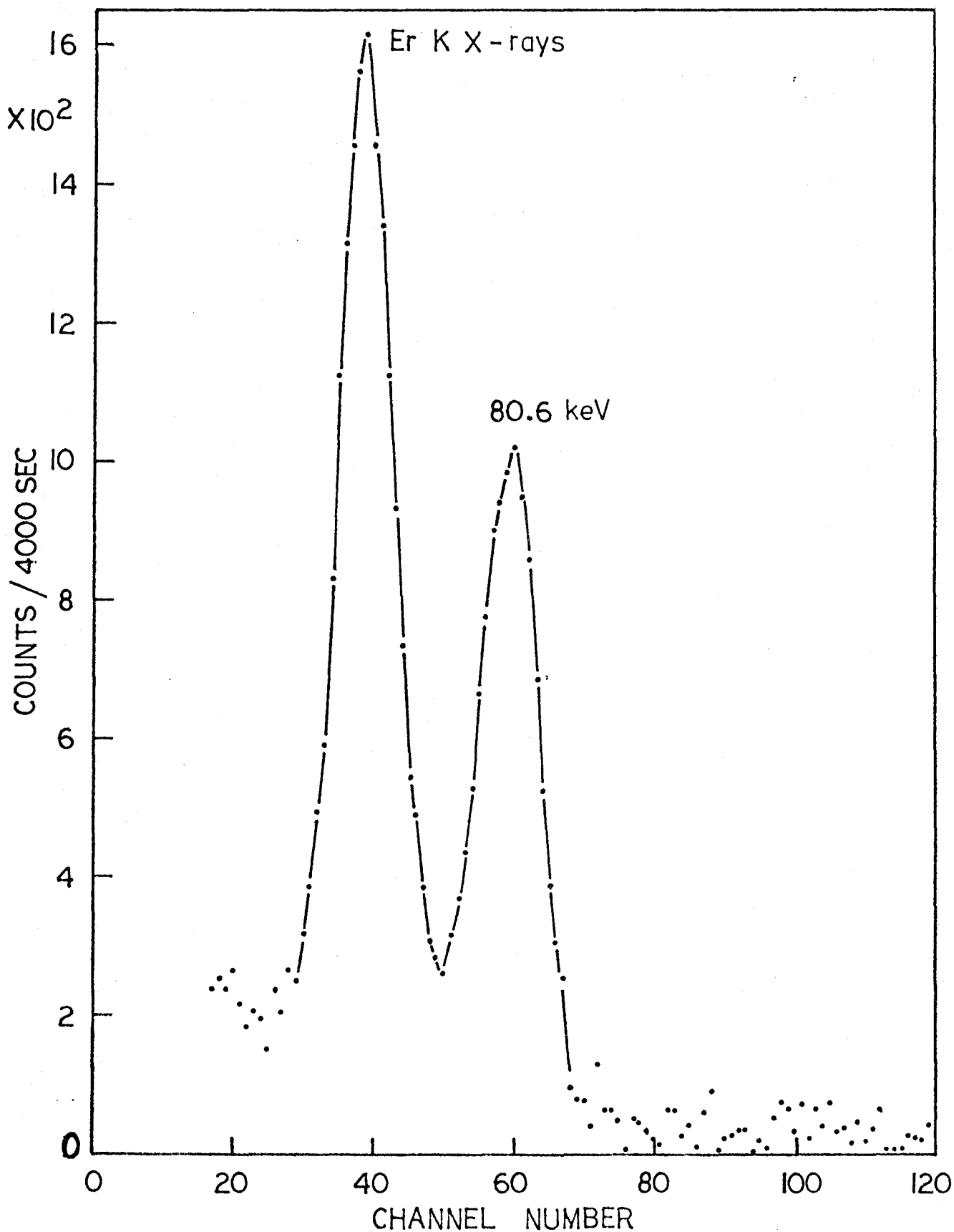
Fig. 19. The NaI(Tl) gamma-ray spectrum of ^{166}Ho.

TABLE 10

Measured and Normalized Mass-Yield
Ratios for Thermal and epi-Sm Fission
of ^{239}Pu (^{166}Dy - ^{166}Ho).

Experiment #	Measured Activity Ratio	Normalized mass-yield ratio (R)	Average % decrease
6	1.68±0.06	1.40±0.07	31±1
7	2.13±0.07	1.50±0.07	

agreement within the experimental error. They were found to be 14.0 ± 0.8 for Mn and 1.98 ± 0.10 for Au.

As mentioned in the previous chapter, a known amount of thorium metal was irradiated under similar condition as for the epi-Sm ^{239}Pu sample. The thorium sample showed mostly activity of 27.4-d ^{233}Pa formed by the activation of ^{232}Th followed by beta decay. However, activities due to fission products from ^{232}Th (fast n, f) reaction could also be identified in the high-resolution Ge(Li) spectrum shown in Fig. 20. The 364.3 keV and 486.8 keV gamma lines associated with ^{131}I and ^{140}La respectively are indicated. Comparison of the results with the epi-Sm sample counted with the same Ge(Li) detector at identical geometry is shown in Table 11. With these data and taking the fast-neutron fission cross-sections of ^{232}Th and ^{239}Pu, and the spectrum of fission neutrons into consideration, it was estimated that ~1% of the total fission events of epi-Sm ^{239}Pu were induced by fast neutrons.
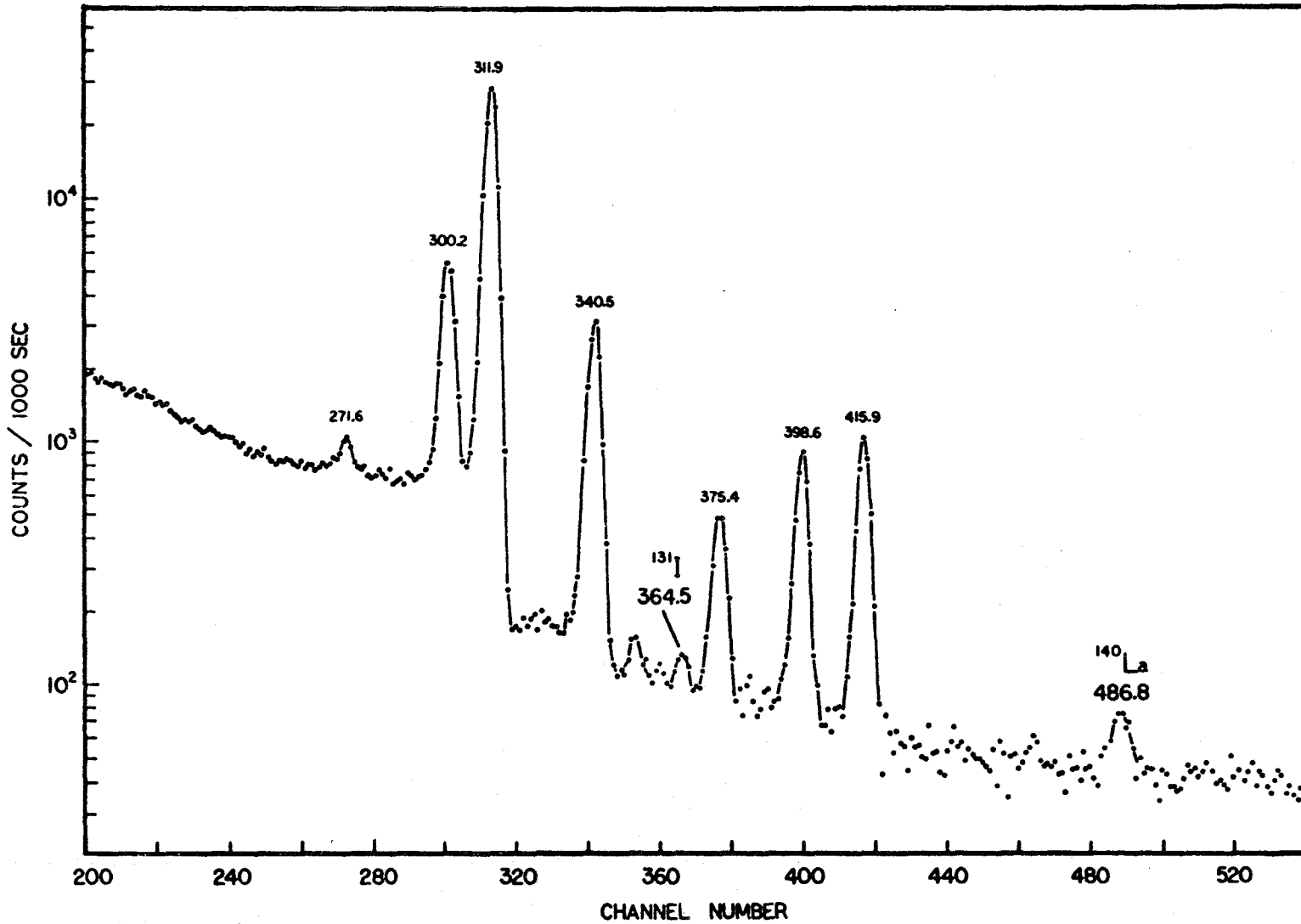
Fig. 20. Ge(Li) gamma-ray spectrum of epi-Sm neutron irradiated ^{232}Th. Gamma-rays from fission products (^{131}I and ^{140}La) are indicated.

81

TABLE 11

Fast-Neutron Fission Contribution Measurement

	^{239}Pu (epi-Sm)	^{232}Th
Sample weight	1.1 mg	24.5 mg
Fast-neutron fission cross-section	2 barns	0.1-0.2 barns
Corrected count rate of ^{131}I (% cumulative mass yield)*	36000 (3.8%)	120 (1.2%)
Corrected count rate of ^{140}La (% cumulative mass yield)*	13000 (5.5%)	130 (6.2%)

* From reference (29).

CHAPTER 4

DISCUSSION

A. Relative Fission Rates of the Low-Energy Resonances in
Thermal, epi-Cadmium and epi-Samarium Fissions of ^{239}Pu

It is of interest to investigate the relative fission
rates of the low energy resonances in the thermal, epi-Cd
and epi-Sm neutron fissions of ^{239}Pu. Such information is useful
in the analysis of the present experimental results. Relatively
crude estimations were carried out because only semiquantitative
interpretations were possible.

It has been shown from the irradiation of metallic thorium
that the contribution of fission induced by fission spectrum neutrons
in the epi-Sm fission ^{239}Pu sample was ~1% of the total fission
events. In addition, Cuninghame et al. [86] reported that the
peak-to-valley mass-yield ratio in terms of ^{99}Mo/^{113}Ag for
1 MeV and 6 Mev neutron-induced fission of ^{239}Pu were 71±9
and 16.7±2 respectively compared with 86 for thermal neutron-
induced fission. Fission contribution due to fission spectrum
neutrons may therefore be neglected in considering the mass
yield variations in the thermal and epi-thermal fissions.

The measured cadmium ratio for the irradiation positions
was 14.0±0.8 for manganese and 1.98±0.10 for gold. According

to the Westcott   convention, the effective cross-section $\hat{\sigma}$

is given in terms of the 2200 m/sec value σ_0 by the relation

$$\hat{\sigma} = \sigma_0 (g+rs)$$

where g and s are factors compiled in reference [87], and r

is a measure of the proportion of epithermal to thermal neutrons

of the reactor neutron spectrum. The value of r may be deduced

from the cadmium ratio measurement. Using a thin detector having

$g \approx 1$ the formula applicable is

$$R_{Cd} = \frac{1 + rs}{r(s + 4\sqrt{kT/\pi E_{Cd}})}$$

where E_{Cd} = cadmium cut off energy, assumed to be 0.67 eV for

a 1 mm thick cadmium cylinder

k = Boltzman constant

and   T = reactor neutron temperature , $\sim 35^\circ C$.

The r value evaluated with the above formula was

0.059. Hence the neutron spectrum can be approximately

represented according to Beckurtz and Wirtz [88] by

$$\Phi(E) = c \left[\frac{E}{(kT)^2} e^{-E/kT} + 0.059\frac{\Delta(E/kT)}{E} \right]$$

where c is a constant characteristic of the total flux and

$\Delta(E/kT)$ is the "joining function" of the thermal flux, represented

by the first term, and the epi-thermal flux, expressed as a

1/E function in the second term.

The joining function $\Delta(E/kT)$ can be either the unit

step $E = \mu kT$ or the function

$$1 / [1 + (\mu kT/E)^{16}]$$

where μ is an integer multiple. Westcott [87] has chosen $\mu = 5$ as a reasonable fit to the theoretical spectra computed for weakly absorbing D_2O media. Since the "joining function" has been observed to depend rather weakly on the properties of the moderator [88], $\mu = 5$ was adopted for the present calculation.

Figure 21 shows the computed neutron spectrum with $c = 2 \times 10^{13}$.

Fission rates of ^{239}Pu as a function of energy can be computed if the fission cross-section function and the neutron spectrum are known. For a ^{239}Pu sample with N_o nuclei of ^{239}Pu per cm^2, the number of interactions is

$$N_I(E) = \Phi(E) [1 - e^{-N_o \sigma_t (E)}]$$

where $\sigma_t(E)$ is the total cross-section. The fission rate is therefore given as

$$R_f(E) = \frac{\sigma_f(E)}{\sigma_t(E)} [1 - e^{-N_o \sigma_t(E)}] \Phi(E)$$

where $\sigma_f(E)$ is the fission cross-section. For $N_o \sigma_t(E) \ll 1$, this formula reduces to

$$R_f(E) \simeq N_o \sigma_f(E) \Phi(E)$$

This approximation is valid for the present calculation with $N_o \sigma_t$ always less than 0.1 and error as high as about 10% permissible for the present purpose.

It is more useful to evaluate fission rates due to
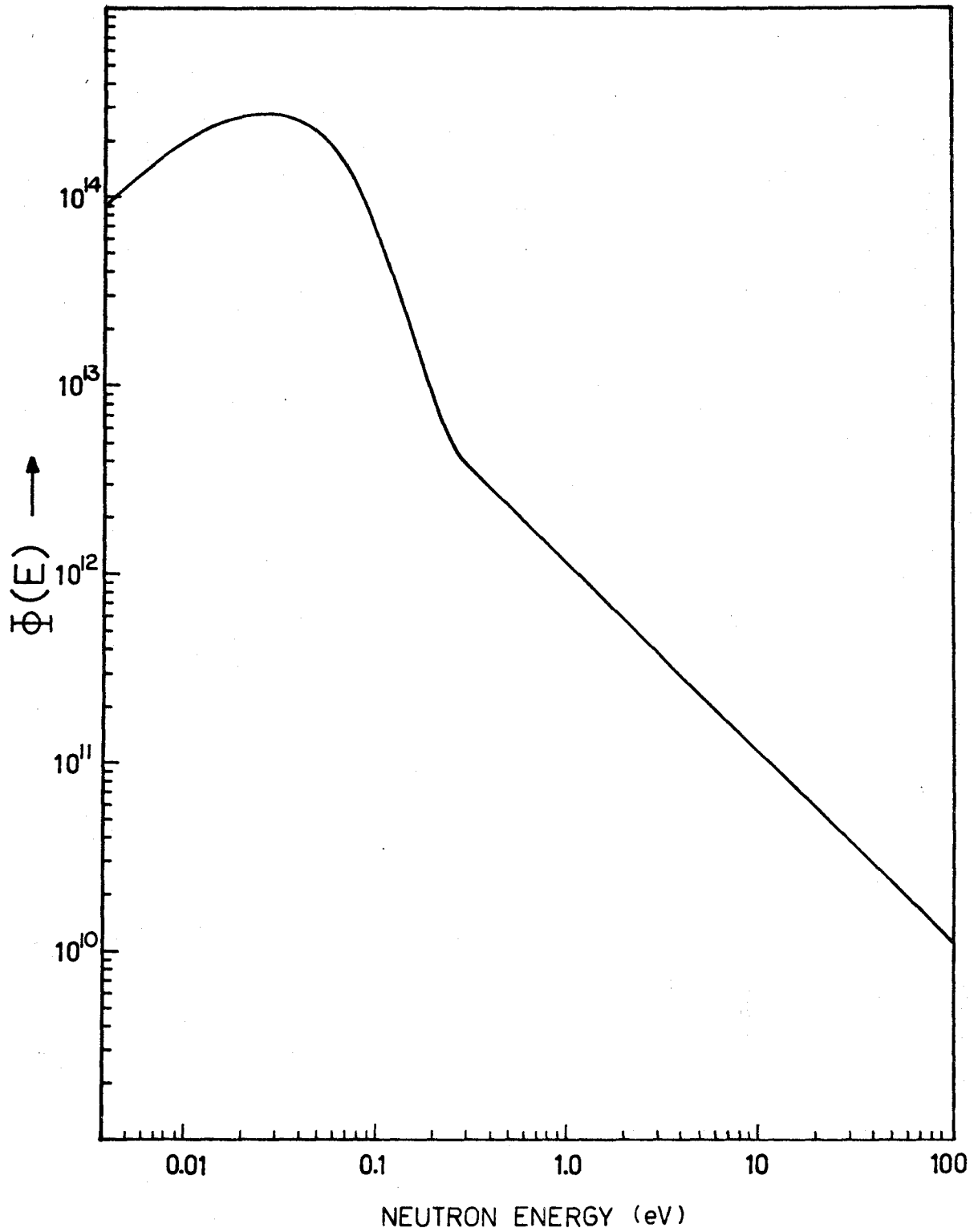
Fig. 21. The reactor neutron spectrum.

different resonances, if the ^{239}Pu fission cross-section can be described in detail in terms of a full set of individual level parameters. According to Lynn[51] this is possible for low energy neutron fissions of ^{239}Pu based on the results of extensive studies by various authors (see (51)). These investigations indicate that the interfernces of the narrow 1^+ levels (constitute about three quarters of the S-Wave levels) and the widely spaced 0^+ levels are negligible. Hence, the total fission cross section $\sigma_f(E)$ can be expressed in terms of the sum of single-level Breit-Wigner terms as

$$\sigma_f(E) = \sum_i \sigma_{fi}(E) = \sum_i 4\pi\lambda^2 \frac{g_{Ji}\Gamma_{ni}\Gamma_{fi}}{4(E-E_{oi})^2 + \Gamma_i}$$

where subscript i refers to the resonance centered at energy E_{oi}, λ is the de Broglie wavelength of the relative motion of neutron and target divided by 2π, Γ_n and Γ_f are the neutron and fission widths respectively, Γ_t is the total width and g_J is a statistical spin factor depending on the total angular momentum J of the compound state. These parameters for resonances up to 260 eV as derived by various authors have been compiled in reference[51] and they are used in the subsequent calculations.

The fission rate due to resonance i is given by

$$R_i = \int_{E_1}^{E_2} N_o\sigma_{fi}(E)\Phi(E)dE$$

where E_1 and E_2 are two limits chosen to give sufficient accuracy in the integration. The R_i values were computed

using different sets of input parameters due to various authors.

Calculations of the relative fission rates of different resonances for the epi-Cd and epi-Sm samples are more complicated. The Cd-and Sm-filtered neutron spectrum as seen by the ^{239}Pu samples is approximately

$$\Phi'(E) = \Phi(E)e^{-n\sigma_{abs}(E)}$$

where $\Phi(E)$ is the unperturbed neutron spectrum, $e^{-n\sigma_{abs}(E)}$ is the transmission factor, n equals the number of Cd or Sm atoms per cm^2 used in shielding, and $\sigma_{abs}(E)$ is the absorption cross-section of Cd or Sm as a function of neutron energy. The fission rate equation for individual resonance then becomes

$$R_i = \int_{E_1}^{E_2} N_o \sigma_{fi}(E)\Phi(E)e^{-n\sigma_{abs}(E)}dE \quad .$$

From the cross-section curve for cadmium[89], we see that only a single-level Breit-Wigner fit for the resonance at 0.178 eV is required for the cross-section expression to be used in the transmission factor. This is given as follows[90]:

$$n\sigma_{abs}(E) = 0.0050762\ell_o/\{\sqrt{E}[4\cdot(E-0.178)^2+0.013112]\}$$

where ℓ_o is the thickness of the cadmium filter in mils , and E in eV.

More resonance terms have to be included in the transmission factor calculation for Sm-filter. In the present evaluation, the input parameters of the resonances involved are listed in Table 12.

Presented in Table 13 are the relative fission rates

TABLE 12

Neutron Capture Resonance Parameters of

Samarium

E_o (eV)	Γ (mV)	Γ_n (mV)	Γ_γ (mV)	J
^{147}Sm (15%)				
3.4	62±5	0.94±0.06	61±5	3
18.3	107±20	66±7	41±17	4
^{149}Sm (13.8%)				
0.0976	63.5±1.0	0.47±0.03	63±1.0	4
0.873	60±1	0.73±0.05	59.8±1.0	4
4.98	68.7±3.0	2.0±0.2	66.7±3.0	4
9.0	74±8	7±3	66.6±6.0	4
Bound level				
^{152}Sm (26.7%)				
8.03	201±8	130±5	71±10	

TABLE 13

Relative Fission Rates of Low Energy Resonance in
the Thermal, epi-Cd and epi-Sm Fissions of ^{239}Pu*

Resonance Energy (eV)	Thermal Fission		Epi-Cd Fission		Epi-Sm Fission	
	Relative Rate	%	Relative Rate	%	Relative Rate	%
-0.26	0.112	35	0.0014	3	0.006	2
0.298	0.225	64	0.0161	30	0.240	87
7.9	0.00064	0.2	0.0064	12	0.0002	0.1
11.0	0.0011	0.3	0.0112	21	0.011	4
11.9	0.00025	0.1	0.0025	5	0.0024	1
14.3	0.00015	<0.1	0.0015	3	0.0015	0.6
14.7	0.00032	0.1	0.0032	6	0.0031	1.2
15.5	0.00037	0.1	0.0027	5	0.0027	1
17.6	0.00026	0.1	0.0026	5	0.0024	1
22.2	0.00028	0.1	0.0028	5	0.0028	1
23.9	0.000007	<0.1	0.00007	0.1	0.00007	<0.1
26.2	0.00011	<0.1	0.0011	2	0.0011	0.4
27.3	0.00001	<0.1	0.0001	0.2	0.0001	<0.1
32.3	0.00001	<0.1	0.0002	0.4	0.0002	<0.1
35.3	0.000001	<0.1	0.00002	<0.1	0.00002	<0.1
41.4	0.00009	<0.1	0.0009	1.6	0.0009	0.3
44.5	0.00005	<0.1	0.0005	0.8	0.0005	0.2
47.6	0.00005	<0.1	0.0006	1.2	0.0006	0.2
	0.351		0.0538		0.276	

* Input resonance parameters are taken fron Bollinger et al.[58].

of the low energy resonances in the thermal, epi-Cd and epi-Sm

fissions of ^{239}Pu, as obtained from the above manipulations.

We note that several authors [51], [54], [58] have

suggested that for the 0.297eV resonance-neutron fission of

^{239}Pu, the compound nucleus should have spin and parity of

1^+, which is different from the"negative energy" resonant states

formed in higher proportion in thermal neutron fission. The

results of Regier et al.[46] indicated that most of the

fissions with epi-Sm neutrons were attributed to the 0.297eV

resonance and they found the prominent variation of the peak-

to-valley mass-yield ratios for epi-Sm neutron compared with

thermal fission was only slightly less than the effect observed

for monochromatic neutrons of 0.297eV.

B. Mass Yield Variations of Asymmetric fissions

Experimental results (Table 7) from careful non-

destructive Ge(Li) spectrometric measurements indicate that

the mass-yield ratios of the asymmetric fission products for

both thermal to epi-Cd and thermal to epi-Sm fissions of ^{239}Pu

remained constant within the limits of statistical errors.

Due to the very high thermal neutron capture cross-section,

the loss in the yield of certain isotope such as ^{135}Xe ($\sigma_c =$

2.7×10^6 barns) has been estimated with the method given in

Appendix A.

Considering the difference in the fission rates of the low energy resonances of the three types of fission (Table 13), these results suggest that the relative yields of the asymmetric fission products do not vary as a function of the spin state of the fissioning compound nucleus. The upper limit of any such effect is estimated to be <5% which is attributed to systematic error of the present measurement. As a matter of fact, this is in agreement with the assumption implied in Wheeler's [51] extension of Bohr's theory [24] in accounting for the variations in the mass-yield ratios of the asymmetric to symmetric fission products.

These results are also consistentwith the two-mode of fission hypothesis, since the relative yields of fission products within the "asymmetric mode" showed no significant fluctuations from one type of fission compared with the other.

It has been mentioned in Chapter 1 that Popa et al. [63] have found significant fluctuations in the relative yields of the asymmetric products from fissions of ^{235}U induced by thermal and epi-Cd neutrons. According to these authors, the relative yields of ^{105}Ru and ^{131}I were much higher (~20%) for epi-Cd fission than for thermal neutron fission, while most of the other nuclides they studied showed less significant changes (Table 14). It seems unlikely that this can be accounted for in terms of shell structure preference; and it is also impossible to relate the result with the observed variations

TABLE 14

Activity Ratios of Fission Products for Thermal to epi-Cd Fission of ^{235}U from Nondestructive Ge(Li) Measurement by Popa et al.[63]

Nuclide	E_γ (keV)	Ratio of Activities (A_{epi-Cd}/A_{th})
^{85m}Kr	151.2	1.00±0.002
^{87}Kr	403	0.94±0.07
^{91m}Y	555.7	0.98±0.02
^{97}Nb	658.1	1.o2±0.015
^{99}Mo-^{99}Tc	181.2	1.05±0.05
^{105}Ru	724.4	1.20±0.09
^{129}Sb	459.6	0.69±0.30
^{131}I	364.5	1.23±0.06
^{132}I	772.8	1.08±0.05
^{133}I	529.6	1.08±0.04
^{135}Xe	249.7	1.04±0.02
^{141}Ba-^{141}La	304.7	1.02±0.04
^{142}La	641.6	0.97±0.05
^{143}Ce	293.2	1.00±0.02
^{146}Pr	453.6	1.00±0.10

in the mass-yield ratios of asymmetric to symmetric fission

products (e.g. results of Faler and Tromp[45]) using Wheeler's

extension of A. Bohr's theory. If such effect was due to the

difference of spin states of the compound nucleus at the

saddle point, the fluctuations would probably be much larger

for ^{239}Pu than for ^{235}U. In actual fact, the results of the

present work on ^{239}Pu exclude such possibility.

C. Mass Yield Variations of Symmetric and Very Asymmetric Fissions

Before discussing the mass yield variations of the

symmetric and very asymmetric fissions there are two points

needed to be taken into consideration. First, the fractional

chain yields of the radiochemically separated nuclides of

^{72}Zn, ^{77}Ge, ^{77}As, ^{112}Pd, ^{115}Cd and ^{166}Dy $-^{166}$Ho of the respective

mass chains have to be evaluated. Results of the estimation

based on the method given in Appendix B showed that the yields

of these nuclides account for over 99% of the chain yields of

the respective chain. Second, because of the high thermal

capture cross-section of 139-min ^{165}Dy (4700 barns), contri-

bution to the total yield of ^{166}Dy from ^{165}Dy (n, γ) has also

been estimated based on method in Appendix A. This was found

to be negligible.

It has been found that the relative mass yields of

asymmetric fission products do not vary significantly for

thermal, epi-Cd and epi-Sm fissions of ^{239}Pu. On this basis,

mass yield variations of some symmetric and very asymmetric fission products were observed. The results are summarized in Table 15 together with experimental data of similar measurements obtained by other authors.

We see that the yield of ^{115}Cd from near symmetric fission of ^{239}Pu decreased by 46±2% in epi-Sm fission as compared with thermal fission. This is somewhat less than the value reported by Regier et al. [46] in which they found a decrease of 60%. The difference is probably due to the fact that Regier et al. had used metallic samarium shielding which is expected to be a more effective filter in cutting off thermal neutrons. The samarium oxide and cement mixture on the other hand might possibly have "windows" arising from non-uniform packing, and also the thick Sm_2O_3-cement (~1cm) shielding could have certain extent of thermalization effects on the penetrating neutron flux.

A similar effect was observed for ^{112}Pd which showed a decrease of 24±3% for the epi-Sm fission compared with thermal fission. Other nuclides in the symmetric region investigated by Regier et al. [46] include ^{121}Sn and ^{125}Sn where they observed decreases of ~55% and 45% respectively.

In general, the more symmetric fission products showed a larger effect and this became decreasingly smaller for less symmetric fission.

For products from very asymmetric fission, a similar

TABLE 15

Summary of the Mass-Yield Ratios for Thermal
to epi-Thermal Fission of ^{239}Pu.

$$\frac{\text{(Yield) Thermal}}{\text{(Yield) epi-Thermal}}$$

Nuclide	Ratio	This Work	%decrease	Fritze[49]	Croall and Willis[48]	Regier et al.[46]
^{72}Zn	Th/Sm	1.44±0.05	30±2			
^{72}Zn	Th/Cd			1.13±0.07		
^{77}Ge	Th/Sm	1.08±0.04				
^{77}Ge	Th/Cd	1.07±0.04				
^{77}As	Th/Cd	1.03±0.04			0.55	
^{78}As	Th/Cd				0.78	
^{111}Ag	Th/Cd				1.07	
^{112}Pd	Th/Sm	1.32±0.08	24±3			
^{113}Ag	Th/Cd				1.38	
^{115}Cd	Th/Sm	1.87±0.08	46±2			2.41±0.15
^{115}Cd	Th/Cd			1.42±0.05		
^{121}Sn	Th/Sm					2.34±0.06
^{125}Sn	Th/Sm					1.79±0.06
^{166}Dy-^{166}Ho	Th/Sm	1.45±0.07	31±2			

trend of effect was observed in this work for ^{72}Zn and ^{166}Ho, the two approximately complimentary fragments formed by the fission of ^{240}Pu compound nucleus. Specifically, the yields of both nuclides were decreased by 30±2% for epi-Sm fission as compared with thermal fission.

Only a very slight decrease was observed for the A = 77 mass chain in the epi-Sm and epi-Cd fissions through careful radiochemical and Ge(Li) spectrometric measurements. This is in contradiction with Croall and Willis' investigation [48] in which they reported considerable increases for both ^{77}As and ^{78}As in the epi-Cd fission. It is to be noted that in the work of these authors who used end-window β-counting, any contamination due to 26-hr ^{76}As formed by ^{75}As (n, γ) would be difficult to resolve from the 38.7-hr ^{77}As. Furthermore, the specific activity produced in the epi-Sm sample of any contamination of natural arsenic would be higher (resonance integral for activation = 36.8 barns) than that could be obtained from the thermal sample (thermal neutron activation cross-section 5.4 ± 1.0 barns). Hence, any contamination of arsenic would cause an increase in the yield of the epi-Cd sample.

In the present work, the high-resolution Ge(Li) gamma counting technique was employed, and it has been proved experimentally that the contamination of ^{77}Ge due to ^{76}Ge (n,γ) is unlikely, especially as an impurity in the aluminum catcher foil.

(1) Interpretation in terms of two-mode of fission hypothesis

The results reported here are in agreement with the two-mode of fission hypothesis of Turkevich and Niday [34], and Fairhall et al.[33], or the so-called "two-component" of Schmitt and Konecny [42] provided one assumes a broad symmetric mode of the gaussian type.

This assumption can be illustrated in Fig. 22 in which the total mass yield curve is represented by the super-position of an asymmetric fission yield curve and a broad symmetric fission yield curve. In order to account for the observed effect in ^{72}Zn and ^{166}Dy $-^{166}Ho$ similar to the effect in symmetric fission, the width of the gaussian "symmetric mode" was estimated to be ~30 mass unit (full width at half maximum, FWHM). The analysis of Britt et al. [37] showed an increase in the width of symmetric mode as a function of increasing mass number of the fissioning nucleus. For ^{226}Ra (13MeV p, f), Schmitt and Konecny [42] have fitted a "symmetric component" for the triple-peaked mass-yield curve with a gaussian of FWHM of 23 mass unit as compared with the FWHM of 17 mass unit for the purely symmetric fission of ^{209}Bi (22MeV d, f) (see reference (33)).

The invoking of the two-mode hypothesis in explaining the mass yield variations requires two separate saddle points with different densities of states in the channel spectra. Businaro and Gallone [91] and Nosoff [92] argued that quadrupole
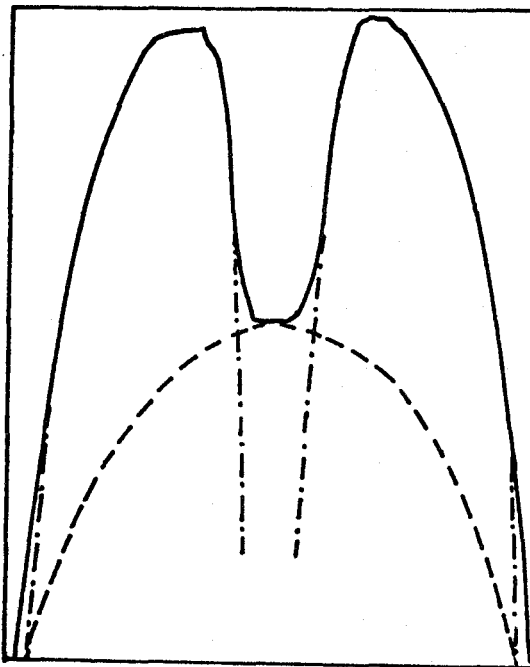
Fig. 22. Decomposition of the fission mass-yield curve (solid line) into two components:

———.———.———.——— "asymmetric component" and

——┬— —— —— —— "symmetric component".

deformations might be expected to lead to a saddle point characteristic of symmetric fission while octupole deformations involve a different saddle point which leads to asymmetric fission. The calculation of Johansson [93] shows that by including shell effects with octupole deformations, the energy levels at large deformations are considerably lowered, leading to an enhancement of asymmetric fission.

This complication seems unnecessary for the description of the mechanism of fission because pertinent experiments (angular distribution measurements) have not indicated more than one saddle point. This is avoided by using the "two-components" of fission of Schmitt and Konecny [42] in which each component may or may not involve different saddle points. Accordingly, the symmetric component is characteristic of a liquid drop while the asymmetric peaks are described by the fragment-structure. As they observed, since the fragments in the symmetric component are formed in softer, relatively highly deformed configurations, it is possible to have a wider range of fission products.

The broad symmetric mode (or component) assumption is not exclusive as far as the present results are concerned. It is also possible that the observed effect is just a consequence of the broadening of the asymmetric fission mass-yield distribution as the yields of symmetric fission is increased.

(2)   Interpretation in terms of the effect of the transition states of the compound nucleus at the saddle point

The review in Chapter 1 suggests that most of the evidences concerning the fission fragment mass, angular and kinetic energy distributions clearly support the channel theory of A. Bohr [24]. That is in the process of fission some constraints are maintained in the transition from saddle point to scission.

The asymmetric to symmetric mass-yield ratios have been observed to vary in a systematic manner from resonance to resonance. Resonances are properties of the compound nucleus. Some property of the saddle point compound nucleus, a certain shape parameter in this case, must still be in effect at the point at which the mass distribution is determined. It has been argued that for low energy neutron fission of ^{239}Pu, the 0^+ resonant states will give rise to a mass-yield distribution with an appreciable amount of symmetric fission, while in the 1^+ resonant states symmetric division is forbidden. We also noted that the 0.297eV resonance might have spin and parity of 1^+ but the negative energy resonance of thermal neutron fission form different states 0^+.

The analysis earlier showed that for thermal fission about ~40% of the fission events occured in the negative energy resonance and about ~60% was due to the 0.297 eV resonance. For epi-Sm fission, negative energy resonance fission contributes very little

while the .297eV resonance fission predominates (85%), with

the rest due to other resonances. Hence the observed decreases

of the symmetric products, 46% in ^{115}Cd and 24% in ^{112}Pd for

epi-Sm fission compared with thermal fission is consistent

with the assignments of 0^+ for the negative energy resonance

and 1^+ for the 0.297eV resonance. And the interpretation

that fission through the 0^+ states has relatively higher yield

for symmetric fission than fission through the 1^+ states is

satisfied. The much smaller fraction of contributions due

to other resonances in the epi-thermal region for both thermal

and epi-Sm fission is a mixture of the two types of resonant

states. The effect of these resonances on the mass yield variations

should therefore be small in comparison with the two with

lowest energies. This is justified if one takes the experi-

mental data of Fritze [49] on the epi-Cd fission of ^{239}Pu into

consideration. Table 13 shows roughly the compositions of

thermal, epi-Sm and epi-Cd fissions of ^{239}Pu where we see that

fissions occur mostly with incident neutron energy greater

than 1eV in the case with cadmium filter. But the mass-yield

variations for ^{115}Cd and ^{72}Zn found by Fritze [49] were

significantly lower than has been found for epi-Sm fission in

this work.

As the mass yields of symmetric fission were decreased,

the products from very asymmetric fissions such as ^{72}Zn and

^{166}Dy-^{166}Ho were also found lowered by 30% in the epi-Sm

fission. The decrease in ^{77}Ge-^{77}As was slight, if any.
Presumably, for fission through the 0^+ resonant states, the
fragments formed in the compound nucleus are soft and highly
deformed so that not only symmetric fission is allowed but
also very asymmetric fission is probable. For fission passing
through the 1^+ resonant states, due to the mass-sloshing
(pear-shaped) mode of collective vibration, the fragments in
the compound nucleus are stiffer because of the preferred
configuration of a core corresponding to a double closed-
shell (N=82, Z=50) being formed in the transition from saddle
point to scission; both symmetric fission and very asymmetric
fission are forbidden.

If the mass distribution is dependent upon the energy
available for deformation and excitation , the spin effect
(corresponding to different modes of motion) would imply
that the heights of the Coulomb barrier at scission must be
different. Moore [94] has pointed out that there are two
possible mechanisms for the transition from the saddle point
to scission. One of these was the proposition of Blyumkina et al.[95]
that the potential energy of collective motion was regarded
to be maintained in the transition and finally changed to
kinetic energy at scission but not available as deformation
energy. The other mechanism viewed the relative separations
of the nascent fragments at scission to be different for
different types of quadrupole or octupole vibrations. This is

expected to be reflected in different shapes or curvatures of the fission barriers for the different channels, as deduced by Vandenbosch [96].

Obviously, the present results are better explained consistently in terms of the second mechanism. Accordingly, the separation of the nascent fragments is larger for fission through 0^+ resonant states than the separation for fission through the 1^+ states. The fragment kinetic energy is therefore expected to be higher for the latter kind of fission.

The idea lends its support from the results of the measurement of Melkonian and Mehta [53] which showed that the variations of fragment energy in low energy neutron fission of ^{239}Pu is correlated with the J-values. Among the 19 levels they studied, 15 levels were found with high average kinetic energy and 4 levels with lower values. The former being assigned J=1 and the latter J=0 (see Table 2) on the basis of the expected ratio of population of the spin states and also for maximum compatibility with other measurements. The neutron multiplicity measurements of Weinstein et al. [54] also agree with such a mechanism. The average neutron yield per fission $(\tilde{\nu}_t)$ in low energy neutron fission of ^{239}Pu was found to be higher for fission through the 0^+ states than through the 1^+ states.

For fission at higher energies, though the correlation between the compound nucleus spin states and the post-scission

characteristics was not established [95-97], the above

mechanism also seems to hold well. Similar arguments have been

invoked by Konecny and Schmitt [42] in the study of ^{226}Ra

(13MeV p, f) to describe the "two fission components", as we

have discussed earlier. Recently, Burnett et al. [98]

have studied the neutron emissions and the total fragment

kinetic energies of ^{233}U (p, f) at proton energies of 13

and 8.5 MeV. The increase in fragment excitation energy at a

prompt fragment of mass ~130 amu was found to be greater than

the increase in excitation energy of the compound nucleus.

The excess excitation energy was compensated by a decrease in

total fragment kinetic energy. The additional excitation energy

was preferentially dissipated to the heavy fragment based on

the variations found in the neutron-yield curves. This view also

tends to be supported by the fact that in the 13 MeV case, the

total fragment kinetic energy is higher at symmetric fission and

lower for asymmetric fission, compared with fission induced

by 8.5 MeV proton.

D. Conclusions

(1) The Ge (Li) spectroscopic measurements indicate

that for high-yield products from asymmetric fission, the

relative yields do not vary significantly for epi-Cd and

epi-Sm fissions of ^{239}Pu as compared with the thermal fission.

This is consistent with the assumptions of both the "two-mode"

(or "two-component") of fission hypothesis, and the extension of the channel theory of A. Bohr often used to interpret the mass-yield variation of symmetric fission as proposed by Wheeler.

(2) The radiochemical measurements observed for epi-Sm fission as compared with thermal fission of ^{239}Pu show (i) marked decreases in the yields of both ^{72}Zn and ^{166}Ho associated with a large decrease in the yield of ^{115}Cd; (ii) the decrease in ^{112}Pd is appreciably less than that of ^{115}Cd, the latter being closer to an exact symmetric division of the compound nucleus; (iii) ^{77}Ge-^{77}As, produced in very asymmetric fission, showed a very slight decrease, if any.

These results are consistent with the "two-mode" or "two-component" of fission hypothesis.

Interpretation in terms of the spin states effect of the compound nucleus at the saddle point is also possible. It is thought that for fission through the 0^+ resonant states, the nascent fragments are formed softer and the heavier fragment is relatively highly deformed and so the distance of separation is larger. Symmetric fission is allowed and very asymmetric fission is also possible. In fission through the 1^+ resonant states, the nascent fragments formed are stiffer, the heavy fragment probably corresponding to a closed-shell structure of Z=50 and N=82 while the inter-fragment separation is shorter. This results in the narrow double-peaked mass distribution.

APPENDIX A

Correction for Neutron Capture Effect

Because of the high neutron capture cross-sections of certain nucleides formed in fission, it is necessary to estimate the effect on the experimental data obtained in this work. Two most prominent cases were considered in the following.

(i) The loss of the yield of ^{135}Xe due to neutron capture reaction during irradiation:

The formation and disappearance of ^{135}Xe can be expressed as follows:

$$^{239}Pu(n,f) \xrightarrow{\ ^{135}y\ } \ ^{135}I \xrightarrow{\ \lambda_1\ } \ ^{135}Xe \underset{\overset{\longrightarrow}{\sigma_c = 2.72 \times 10^6 \ barns}}{\overset{\lambda_2}{\longrightarrow}} \begin{matrix} ^{135}Cs \\ \\ ^{136}Xe \end{matrix}$$
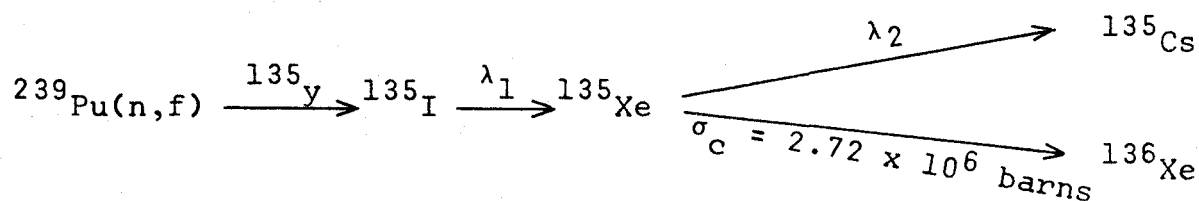
where ^{135}y is the cumulative yield of ^{135}I in fission, λ_1 and λ_2 are decay constants of ^{135}I and ^{135}Xe respectively, and σ_c is the thermal neutron capture cross-section of ^{135}Xe.

The rate of formation of ^{135}I is given by

$$\frac{dN_i(I)}{dt} = \ ^{135}yN_{Pu}\sigma_{f,Pu}\phi - N_i(I)\lambda_1 \qquad (1)$$

where $^{135}yN_{Pu}\sigma_{f,Pu}\phi = R_f\ ^{135}y$ = rate of production of ^{135}I from fission,

N_{Pu} = number of ^{239}Pu in sample,

σ_f = fission cross-section of ^{239}Pu,

and ϕ = thermal neutron flux.

The rate of formation of ^{135}Xe is given as

$$\frac{dN_i(Xe)}{dt} = N_i(I)\lambda_1 - N_i(Xe)\lambda_2 - N_i(Xe)\sigma_c\phi \tag{2}$$

The independent yield of ^{135}Xe from fission was assumed to be negligible based on the estimation made according to Appendix B.

The solutions of differential equations (1) and (2) are:

$$N_i(I) = \frac{^{135}yR_f}{\lambda_1}(1 - e^{-\lambda_1 t})$$

and

$$N_i(Xe) = \frac{^{135}yR_f}{\lambda_2+\sigma_c\phi}\left[1 + \frac{\lambda_2+\sigma_c\phi}{\lambda_1-\lambda_2-\sigma_c\phi}e^{-\lambda_1 t} - \frac{\lambda_1}{\lambda_1-\lambda_2-\sigma_c\phi}e^{-(\lambda_2+\sigma_c\phi)t}\right]$$

If $\sigma_c\phi = 0$,

$$N_i'(Xe) = \frac{^{135}yR_f}{\lambda_2}\left[1 + \frac{\lambda_2}{\lambda_1-\lambda_2}e^{-\lambda_1 t} - \frac{\lambda_1}{\lambda_1-\lambda_2}e^{-\lambda_2 t}\right]$$

However, at the time of gamma-ray counting with Ge(Li) detector, a large proportion of ^{135}Xe would have been formed from the decay of ^{135}I during the cooling period of the sample through the sequence below,

$$^{135}I \xrightarrow{\lambda_1} {}^{135}Xe \xrightarrow{\lambda_2} {}^{135}Cs$$
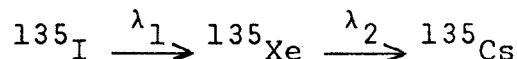
for which

$$N_f(Xe) = \frac{\lambda_1}{\lambda_2-\lambda_1}N_i(I)(e^{-\lambda_1 t} - e^{-\lambda_2 t}).$$

From the relative values of $N_i(Xe)$, $N_i'(Xe)$ and $N_f(Xe)$ at the time of radio-counting, the loss of the yield

of ^{135}Xe due to neutron capture reaction in the thermal fission sample of ^{239}Pu can be corrected and this was ~6% of the total count rates.

(ii) The contribution of ^{165}Dy$(n,\gamma)^{166}$Dy to the final yield of ^{166}Dy. Consider the reactions,

$$^{239}\text{Pu(n,f)} \xrightarrow{\;^{165}y\;} {}^{165}\text{Dy} \underset{\underset{\sigma_c = 4700\,b}{(n,\gamma)}}{\overset{\lambda_1}{\Bigg\langle}} \begin{array}{c} ^{165}\text{Ho} \\[2ex] ^{166}\text{Dy} \xrightarrow{\lambda_2} {}^{166}\text{Ho} \end{array} \qquad (3)$$

and

$$^{239}\text{Pu(n,f)} \xrightarrow{\;^{166}y\;} {}^{166}\text{Dy} \xrightarrow{\;\lambda_2\;} {}^{166}\text{Ho} \qquad (4)$$

for which the following differential equations are obvious,

$$\frac{dN_f(165)}{dt} = {}^{165}yR_f - N_f(165)\lambda_1 - N_f(165)\sigma_c\phi \qquad (5)$$

$$\frac{dN_c(166)}{dt} = N_f(165)\sigma_c\phi - N_c(166)\lambda_2 \qquad (6)$$

and

$$\frac{dN_f(166)}{dt} = {}^{166}yR_f - N_f(166)\lambda_2 \qquad (7)$$

where subscripts 'c' and 'f' refer to capture and fission contributions, while the symbols have usual significance as in case (i). The solutions are given as:

$$N_f(165) = \frac{{}^{165}yR}{\lambda_1 + \sigma_c\phi}\left[1 - e^{-(\lambda_1 + \sigma_c\phi)t}\right]$$

$$N_f(166) = \frac{{}^{166}yR}{\lambda_2}\left[1 - e^{-\lambda_2 t}\right]$$
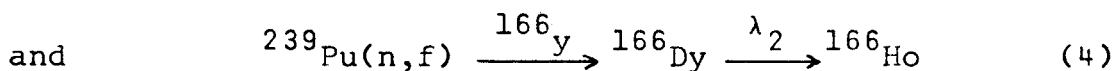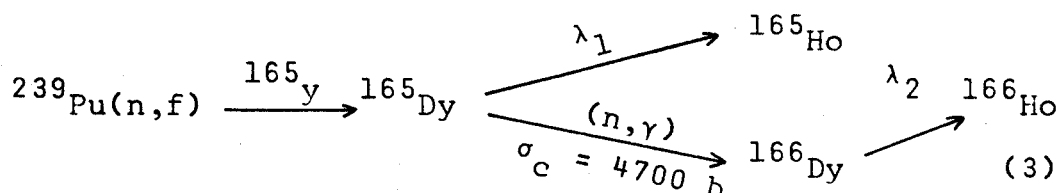
and

$$N_c(166) = \frac{\sigma_c\phi\,^{165}yR_f}{\lambda_1 + \sigma_c\phi}\left[\frac{1}{\lambda_2} + \frac{e^{-(\lambda_1 + \sigma_c\phi)t}}{\lambda_1 + \sigma_c\phi - \lambda_2}\right.$$

$$- \frac{\lambda_1 + \sigma_c \phi}{\lambda_2 (\lambda_1 + \sigma_c \phi - \lambda_2)} \ e^{-\lambda_2 t} \ \Biggr]$$

By substitution of the appropriate values, the ratio of ^{166}Dy formed by fission to that formed by neutron capture of ^{165}Dy after an irradiation period of 20 hours is

$$\frac{N_f(166)}{N_c(166)} \approx 1/400.$$

APPENDIX B

Calculation of the Fractional Chain Yield

Approximate fractional chain yields can be obtained by the method of Coryell et al. [99]. These authors assumed that the equal charge displacement hypothesis and the well-established shape of the charge distribution curve along any isobaric sequence for the thermal fission of ^{235}U are generally valid for fissions differing in compound nucleus and excitation energy.

The following expression which uses the Z_p (most probable charge) function of the thermal fission of ^{235}U as reference, was derived for computing the value of Z_p of any mass number A for the fission of a compound nucleus with atomic number Z_c, and mass number A_c:

$$Z_p(A) - Z_p(A)^{235} = \Delta Z_p(A)$$
$$\Delta Z_p(A) = \frac{1}{2}(Z_c - 92) - 0.21(A_c - 236) + 0.19(\nu_t - \nu_t^{235})$$

where ν_t is the average number of neutrons emitted per fission. With $\nu_t^{235} = 2.43$ and $\nu_t(^{239}Pu) = 2.87$ [5], the Z_p function for the thermal fission of ^{239}Pu is given as:

$$Z_p(A) = Z_p(A)^{235} + 0.32.$$

The fractional chain yield of a specific nuclide with atomic number Z of an isobaric sequence is then

evaluated by applying the empirical charge dispersion
formula:

$$P(Z) = (1/\sqrt{c\pi}) \exp (-(Z-Z_p)^2/c)$$

where $c = 0.80 \pm 0.14$ according to a recent publication of
Wahl et al. [9]. This Gaussian distribution is normalized
so that the sum of all points taken at unit intervals is
unity.

Cumulative fractional chain yield of a nuclide
(Z,A) is obtained by summing the fractional chain yields
of itself and its precursors. In this way, using the
$Z_p(A)^{235}$ values compiled by Wahl et al. [9], the cumulative
fractional chain yields of ^{72}Zn, ^{77}As, ^{112}Pd, ^{115}Cd and
^{166}Dy were found to represent over 99% of the total yields
of the respective mass chain. The sum of the fractional
chain yields of ^{77}Ge and ^{77m}Ge also amounts over 99%.

REFERENCES

1. O. Hahn and F. Strassmann, Naturwiss. <u>27</u>, 11, 89 (1939).

2. L. Meitner and O. R. Frisch, Nature <u>143</u>, 239, 471 (1939).

3. N. Bohr and J. A. Wheeler, Phys. Rev. <u>56</u>, 426 (1939).

4. C. D. Coryell and N. Sugarman (editors), "Radiochemical Studies: The Fission Products". Nat. Nucl. Energy Ser., Division IV, Plutonium Project Record, Vol. 9 (New York: McGraw-Hill Book Company, 1951).

5. E. K. Hyde, "The Nuclear Properties of the Heavy Elements", Vol. III: Fission Phenomena. Prentice-Hall, Englewood Cliffs, New Jersey (1964).

6. J. C. D. Milton and J. S. Fraser, "Nuclear Fission", Ann. Rev. Nucl. Sci. (1966).

7. J. E. Gindler and J. R. Huizenga, "Nuclear Chemistry", Vol. II, p. 2, L. Yaffe (Editor), Academic Press (1968).

8. L. E. Glendenin, C. D. Coryell and R.R. Edwards, Distribution of Nuclear Charge in Fission, Paper 52 in Reference (4).

9. A. C. Wahl, A. E. Norris, R. A. Rouse and J. C. Williams, Proceedings of the Second Symposium on Physics and Chemistry of Fission, Paper IAEA-SM-122/116, Vienna (1969).

10. S. Cohen and W. J. Swiatecki, Ann. Phys. <u>19</u>, 67 (1962).

                                                  <u>22</u>, 406 (1963).

11. V. M. Strutinskii, N. Ya. Lyashchenko and N. A. Popov, JETP (Sov. Phys.) $\underline{16}$, 418 (1963).

12. D. L. Hill and J. A. Wheeler, Phys. Rev. $\underline{89}$, 1102 (1953).

13. J. R. Nix, Nucl. Phys. $\underline{A130}$, 241 (1969).

14. V. M. Strutinsky, Nucl. Phys. $\underline{A95}$, 420 (1965).

15. S. Bjørholm and V. M. Strutinsky, Nucl. Phys. $\underline{A136}$, 1 (1969).

16. P. Fong, Phys. Rev. $\underline{102}$, 434 (1956).

17. J. K. Perring and J. S. Storey, Phys. Rev. $\underline{98}$, 1525 (1955).

18. P. Fong, Phys. Rev. $\underline{135}$, B1338 (1964).

19. W. Brunner and H. Paul, Ann. Physik. $\underline{6}$, 267 (1960).

    ————— $\underline{7}$, 326 (1961).

    ————— $\underline{7}$, 333 (1961).

    ————— 8, 146 (1961).

20. T. D. Thomas and R. Vandenbosch, Phys. Rev. $\underline{133}$, B976 (1964).

21. R. Ramanna R. Subramanian and R. N. Aiyer, Nucl. Phys. $\underline{67}$, 529 (1965).

22. L. Wilets, "Theories of Nuclear Fission", Clarendon Press, Oxford (1964).

23. W. J. Swiatecki, Paper SM-60/1, Proceedings of Symposium on Physics and Chemistry of fission, Salzburg, 1965, (Vienna) Vol. 1, p. 3.

24. A. Bohr, Proceedings of the Int. Conf. on the Peaceful Uses of Atomic Energy, Geneva, 1955 (United Nations, New York, 1956), Vol. 2, p. 151.

25. H. Faissner and K. Wildermuth, Nucl. Phys. $\underline{58}$, 177 (1964).

26. J. J. Griffin, Proceedings of the Second Symposium on Physics and Chemistry of Fission , Paper IAEA-SM-122/200, IAEA, Vienna (1969).

27. I. Halpern and E. M. Henley, Comments on Nuclear and Particle Physics, V. III, Number 2, 52 (1969).

28. N. Feather, Proceedings of the Second Symposium on Physics and Chemistry of Fission , Paper IAEA-SM-122/201, Vienna (1969).

29. S. Katcoff, Nucleonics $\underline{18}$, 201 (1960).

30. H. G. Thode and R. L. Graham, Can. J. Research $\underline{25A}$, 1 (1947).

    R. K. Wanless and H. G. Thode, Can. J. Phys. $\underline{33}$, 541 (1955).

    H. Farrar and R. H. Tomlinson, Can. J. Phys. $\underline{40}$, 943 (1962).

31. R. B. Levy, H. G. Hicks, W. E. Nervik, P. C. Stevenson, J. B. Niday and J. C. Armstrong, Jr., Phys. Rev. $\underline{124}$, 544 (1961).

32. N. I. Borisova, S. M. Dubrovia, V. I. Novgorodtseva, V. A. Pchelin, V. A. Shigin and V. M. Shubko, Sov. J. of Nucl. Phys. (English) $\underline{6}$, 331 (1967).

33. A. W. Fairhall, R. C. Jensen and E. F. Neuzil, paper P/677, Proc. of the 2nd U.N. Conf. on the Peaceful Uses of Atomic Energy $\underline{15}$, Geneva (1958).

34. A. Turkevich and J. B. Niday, Phys. Rev. <u>84</u>, 52 (1951).

35. L. J. Colby, M. La Salle-Shouf and J. Cobble, Phys. Rev. <u>121</u>, 1415 (1961).

36. R. H. Iyer <u>et al</u>., J. Inorg. Nucl. Chem. <u>25</u>, 465 (1963).

37. H. C. Britt and S. L. Whetstone, Jr., Phys. Rev. <u>133</u>, B603 (1964).
    H. C. Britt, H. E. Wegner and J. C. Gursky, Phys. Rev. <u>129</u>, 2239 (1963).

38. G. P. Ford, Phys. Rev. <u>118</u>, 1261 (1960).

39. H. G. Hicks, H. B. Levy, W. E. Nervik, P. C. Stevenson, J. B. Niday and J. C. Armstrong, Jr., Phys. Rev. <u>128</u>, 700 (1962).

40. G. P. Ford and R. B. Leachman, <u>In</u> "Physics and Chemistry of Fission", Vol. 1, p. 333, IAEA, Vienna (1965).

41. G. R. Choppin and E. F. Meyer, Jr., J. Inorg. Nucl. Chem. <u>28</u>, 1509 (1966).

42. E. Konecny and H. W. Schmitt, Phys. Rev. <u>172</u>, 1213 (1968).

43. J. R. Nix and W. J. Swiatecki, Nucl. Phys. <u>71</u>, 1 (1965).

44. Los Alamos Radiochemistry Group, Phys. Rev. <u>107</u>, 325 (1957).

45. K. T. Faler and R. L. Tromp, Phys. Rev. <u>131</u>, 1746 (1963).

46. R. B. Regier, W. H. Burgus, R. L. Tromp and B. H. Sorenson, Phys. Rev. <u>119</u>, 2017 (1960).

47. G. A. Cowan, B. P. Bayhurst and R. J. Prestwood, Phys. Rev. 130, 2380 (1963).

G. A. Cowan, B. P. Bayhurst, R. J. Prestwood, J. S. Gilmore and G. W. Knobeloch, Phys. Rev. 144, 979 (1966).

————— Phys. Rev. C 2, 615 (1970).

48. J. F. Croall and H. H. Willis, In "Physics and Chemistry of Fission", Vol. I, p. 355, IAEA, Vienna (1965).

49. K. Fritze, Radiochim. Acta 5, 57 (1966).

50. J. A. Wheeler, Physica 22, 1103 (1956).

—————, In "Fast Neutron Physics" (J. B. Marion and J. L. Fowler, eds.) Part 2, p. 2051, Interscience, New York (1963).

51. J. E. Lynn, "Theory of Neutron Resonance Reactions", Clarendon Press, Oxford, 1968.

52. J. J. Griffin, In "Physics and Chemistry of Fission", Vol. I, p. 23, IAEA, Vienna (1965).

53. E. Melkonian and G. K. Mehta, In "Physics and Chemistry of Fission", Vol. II, p. 355, IAEA, Vienna (1965).

54. S. Weinstein, R. Reed and R. C. Block, "Proceedings of the Second Symposium on Physics and Chemistry of Fission", p. 477, IAEA, Vienna (1969).

55. M. Asghar, A. Michaudon, and D. Payer, Phys. Lett. 26B, 664 (1964).

56. H. Weigman, J. Winter and M. Heske, Nucl. Phys. A134, 535 (1969).

57. C. D. Bowman, J. Berman and R. Bagham, WASH-1127, Comp. by M. S. Moore (1969).

58. L. M. Bollinger, R. E. Cote and G. E. Thomas, In "Proceedings of the Second Int. Conf. on the Peaceful Uses of Atomic Energy", Vol. 15, p. 127, United Nations, Geneva (1958).

59. G. D. Sauter and C. D. Bowman, Phys. Rev. Lett. $\underline{15}$, 761 (1965).

60. T. J. King and R. C. Block, Nucl. Phys. $\underline{A138}$, 556 (1969).

61. M. Asghar, Nucl. Phys. $\underline{A98}$, 33 (1967).

62. J. A. Farrell, Phys. Rev. $\underline{165}$, 1371 (1968).

63. P. Popa, M. De. Coster and P. H. M. Van Assche, Nucl. Sci. Eng. $\underline{39}$, 50 (1970).

64. G. E. Gordon, J. W. Harvey and H. Nakahara, Nucleonics $\underline{24}$, 62 (1966).

65. L. Wish, Phys. Rev. $\underline{172}$, 1262 (1968).

66. G. M. Lederer, J. M. Hollander and I. Perlman, "Table of Isotopes", sixth edition, John Wiley & Sons (1967).

67. A. Ng, Phys. Rev. $\underline{176}$, 1329 (1968).

68. D. J. Gorman, Ph.D. Thesis, McMaster University (1967).

69. J. Korkisch, "Modern Method for the Separation of Rarer Metal Ions", Oxford, New York, Pergamon Press (1969).

70. J. L. Ryan and E. J. Wheelwright, Proceedings of 2nd Int. Conf. on the Peaceful Uses of Atomic Energy, United Nations, Geneva (1958), Vol. 17, p. 137.

71. I. M. Kolthoff and P. J. Elving (editors), "Treatise on Analytical Chemistry", N.Y., Part II, Vol. 9, p. 283 (1962).

72. H. G. Hicks, The Radiochemistry of Zinc, NAS-NS3015 (1960).

73. O. T. Hogdahl, The Radiochemistry of Palladium, NAS-NS3052 (1961).

74. J. De Voe, The Radiochemistry of Cadmium, NAS-NS3001 (1960).

75. H. C. Beard, The Radiochemistry of Arsenic, NAS-NS3002 (1960).

    J. A. Marinsky, The Radiochemistry of Germanium, NAS-NS3043 (1961).

    I. F. Croall and H. H. Willis, AERE-R4723 (1964).

76. W. F. Hillebrand, G. E. F. Lundell, H. A. Bright and J. I. Hoffman, "Applied Inorganic Analysis", John Wiley & Sons, New York (1953).

77. P. C. Stevenson and W. E. Nervik, The Radiochemistry of the Rare Earths, Scandium, Yttrium and Actinium, NAS-NS3020 (1961).

78. G. R. Choppin and R. J. Silva, J. Inorg. Nucl. Chem. 3, 153 (1956).

79. H. L. Smith and D. C. Hoffman, J. Inorg. Nucl. Chem. 3, 243 (1956).

80. J. Minzewski and R. Dybezinski, J. of Chromatog. 7, 98 (1962).

81. I. P. Alimarin, Yu. V. Jekolev, A. Z. Miklishanky, N. N. Dogadkin and O. V. Stepanets, J. Radioanal. Chem. $\underline{1}$, 139 (1968).

82. K. Wolfsberg, Anal. Chem. $\underline{34}$, 518 (1962).

83. W. W. Wendlandt, Anal. Chem. $\underline{31}$, 408 (1959).

84. R. C. Vickery, "Analytical Chemistry of the Rare Earths", Oxford, New York, Pergamon Press (1961).

85. R. L. Heath, "Modern Trends in Activation Analysis", J. R. De Voe (Editor), NBS Special publ. 312, Vol. II, p. 959 (1969).

86. J. G. Cuninghame, K. Fritze, J. E. Lynn and C. B. Webster, Nucl. Phys. $\underline{84}$, 49 (1966).

87. C. H. Westcott, CRRP-680 (1957).

_____, AECL-1101 (1962).

88. K. H. Beckurtz and K. Writz, "Neutron Physics", Springer-Verlag, N.Y. (1964).

89. D. J. Hughes and J. A. Harvey, "Neutron Cross-Sections", BNL-325 (1958).

90. R. W. Stoughton and J. Halperin, Nucl. Sci. Eng. $\underline{15}$, 314 (1963).

91. U. L. Businaro and S. Gallone (1955), Nuovo Cimento $\underline{1}$, 629 (1955).

92. V. G. Nossoff, In "Proc. of the 1st Int. Conf. on the Peaceful Uses of Atomic Energy", Vol. 2, p. 205, United Nations, New York (1956).

93. S. A. E. Johansson, Nucl. Phys. $\underline{22}$, 529 (1961).

94. M. S. Moore, IN-1222 (1969).

95. Yu. A. Blyumkina I. I. Bondarenko, V. F. Kuznetsov,

     V. G. Nesterov, V. N. Okolovitch, G. N. Smirenkin and

     L. N. Usachev, Nucl. Phys. $\underline{52}$, 648 (1964).

96. R. Vandenbosch, Nucl. Phys. $\underline{A101}$, 460 (1967).

97. J. G. Cuninghame, G. P. Kitt and F. R. Rae, Nucl.

     Phys. $\underline{27}$, 154 (1961).

98. S. C. Burnett, R. L. Ferguson, F. Plasil and

     H. W. Schmitt, Phys. Rev. C $\underline{3}$, 2034 (1971).

99. C. D. Coryell, M. Kaplan and R. D. Fink, Can. J. Chem.

     $\underline{39}$, 646 (1961).